Title: Inflammation and matrix metalloproteinase 9 (Mmp-9) regulate photoreceptor regeneration in adult zebrafish

Abbreviated Title: Inflammation in zebrafish tissue regeneration

Authors: Nicholas J. Silva[1, 2], Mikiko Nagashima[2], Jingling Li[3], Laura Kakuk-Atkins[2], Milad Ashrafzadeh[2], David R. Hyde[3], Peter F. Hitchcock[1, 2]

1. Neuroscience Graduate Program, University of Michigan, Ann Arbor, MI 48109
2. Department of Ophthalmology and Visual Sciences, University of Michigan, Ann Arbor, MI 48105
3. Department of Biological Sciences, University of Notre Dame, Notre Dame, IN, 46556

Corresponding Author:

Peter F. Hitchcock
University of Michigan
Department of Ophthalmology and Visual Sciences
W.K. Kellogg Eye Center
1000 Wall Street
Ann Arbor, MI 48105
peterh@med.umich.edu
734-763-8169

Number of Pages: 37

Number of Figures: 12 + 1 figure in Extended Data

Number of Tables: 2

Number of Words – Abstract: 156

Number of Words – Introduction: 698

Number of Words – Discussion: 1420

Acknowledgements:
This work was supported by grants from the National Institutes of Health - R01EY07060 (PFH), R01 EY024519 (DRH), T32EY013934 (NJS), P30EYO7003 (PFH) and an unrestricted grant from the Research to Prevent Blindness, New York. The authors thank Dilip Pawar for technical assistance. Fish lines and reagents provided by ZIRC were supported by NIH-NCRR Grant P40 RR01.

Conflict of Interest Statement:

The authors declare no competing financial interests.

Abstract

Brain injury activates complex inflammatory signals in dying neurons, surviving neurons, and glia. Here, we establish that inflammation regulates the regeneration of photoreceptors in the zebrafish retina and determine the cellular expression and function of the inflammatory protease, matrix metalloproteinase 9 (Mmp-9), during this regenerative neurogenesis. Animals of either sex were used in this study. Following photoreceptor ablation, anti-inflammatory treatment suppresses the number of injury-induced progenitors and regenerated photoreceptors. Upon photoreceptor injury, *mmp-9* is induced in Müller glia, the intrinsic retinal stem cell, and Müller glia-derived photoreceptor progenitors. Deleting *mmp-9* results in over production of injury-induced progenitors and regenerated photoreceptors, but over time the absence of Mmp-9 compromises the maturation and survival of the regenerated cones. Anti-inflammatory treatment in mutants rescues the defects in cone maturation and survival. These data provide a link between injury-induced inflammation in the vertebrate CNS, Mmp-9 function during photoreceptor regeneration and the requirement of Mmp-9 for the survival of regenerated cones.

Significance Statement

The innate immune system is activated by neuronal death, and recent studies demonstrate that in zebrafish neuroinflammation is required for neuronal regeneration. The roles of inflammatory cytokines are being investigated, however, the function of the inflammatory protease, matrix metalloprotease Mmp-9, in neuronal regeneration is unknown. We show herein that in adult zebrafish retinal inflammation governs the proliferative phase of the stem cell-based regeneration of rod and cone photoreceptors and determine the specific roles for Mmp-9 in photoreceptor regeneration. This study provides the first mechanistic insights into the potential role of Mmp-9 in retinal regeneration and serves to link neuroinflammation, stem cell-based regeneration of photoreceptors and human photoreceptor disease.

102 **Introduction**

103 Inflammation modulates immune and nonimmune functions during tissue development, repair,
104 and diseases (Deverman and Patterson, 2009; Ekdahl et al., 2009). Acute inflammation involves
105 the secretion of proinflammatory cytokines and chemokines that recruit immune cells to the
106 damaged tissue (Liddiard et al., 2011; Nathan, 2002). In the central nervous system of adult
107 mammals, acute inflammation can activate signaling cascades in stem and progenitor cells that
108 stimulate proliferation and promote neurogenesis (Borsini et al., 2015; Ekdahl et al., 2009; Kizil
109 et al., 2015; Kyritsis et al., 2014, 2012). Chronic inflammation, however, is detrimental, and
110 results in secondary damage to neurons and, in severe cases, neurodegenerative disease
111 (Amor et al., 2010). Proper regulation of the inflammatory cascades in the central nervous
112 system is critical both to maintain tissue homeostasis and successfully repair brain injuries.

113 Unlike mammals, which possess a limited capacity for tissue regeneration, zebrafish
114 have an astonishing ability to regenerate tissues and organs, such as fins, heart, brain, and
115 retina (Gemberling et al., 2013; Kizil et al., 2012; Lenkowski and Raymond, 2014). Studies using
116 zebrafish have identified cellular and molecular mechanisms which may unlock the regenerative
117 potential of mammalian tissues (Ueki et al., 2015). Such mechanisms include inflammation. In
118 zebrafish acute inflammation is both necessary and sufficient to induce neuronal regeneration
119 (Kyritsis et al., 2012; White et al., 2017; Caldwell et al., 2019).

120 In the zerbrafish retina, Müller glia serve as intrinsic stem cells that underlie the ability to
121 regenerate retinal neurons (Bernardos et al., 2007; Fausett and Goldman, 2006). Neuronal
122 injury and death stimulate Müller glia to initiate a transient gliotic response, followed by partial
123 dedifferentiation and entry into the cell cycle (Raymond et al., 2006; Thomas et al., 2016).
124 Müller glia then undergo a single asymmetric division to produce multipotent progenitors, which
125 proliferate rapidly, migrate to areas of cell death and differentiate to replace the ablated neurons
126 (Fimbel et al., 2007; Sherpa et al., 2008; Goldman, 2014; Gorsuch and Hyde, 2014; Lenkowski
127 and Raymond, 2014). In the zebrafish retina, paracrine and autocrine signaling that engage

128 Müller glia plays an essential role facilitating this regenerative neurogenesis (Nelson et al.,
129 2013; Zhao et al., 2014). Following a photolytic lesion, dying photoreceptors secrete Tnf-α, to
130 which Müller glia respond by partial dedifferentiation, synthesis of Tnf–α and entry into the cell
131 cycle (Nelson et al., 2013). Mechanical lesions induce the expression of *leptin* and Il-6 family
132 cytokines in Müller glia and Müller glia-derived progenitors and is required for injury-induced
133 proliferation (Zhao et al., 2014).

134 Matrix metalloproteinase 9 (Mmp-9) is a secreted protease that plays a prominent role in
135 tissue development and homeostasis by acting on extracellular molecules, including adhesion
136 molecules, growth factors and cytokines (Bonnans et al., 2014; Le et al., 2007; Masure et al.,
137 1991; Parks et al., 2004; Vandooren et al., 2013b, 2014), which, in turn, can regulate
138 proliferation, cellular migration and cellular differentiation. It is well established that inflammatory
139 cytokines can induce the expression of MMPs, including MMP-9 (Vecil et al., 2000; Shubayev et
140 al., 2006; Nagase, et al., 2006; Vandooren, et al., 2013b). MMP-9 was first purified from
141 neutrophils and monocytes following stimulation by IL-8 and IL-1β, implicating its role as an
142 inflammatory protease (Masure et al. 1991; Opdenakker, et al., 1991). In adult tissues, Mmp-9 is
143 dramatically induced following various types of injuries (Vandooren et al., 2013b, 2014; Xu et
144 al., 2018). The complexities of Mmp-9 function suggest its role during regeneration is likely
145 tissue, substrate and injury context dependent (Hindi et al., 2013; Vandooren et al., 2014; Ando
146 et al., 2017; Xue et al., 2017). The cellular expression and function of Mmp-9 during
147 photoreceptor regeneration in the zebrafish are unknown.

148 Here, we determine the general role of inflammation and the cellular expression and
149 function of the matrix metalloproteinase, Mmp-9, during photoreceptor regeneration. We
150 establish that in the adult retina inflammation governs the proliferation of Müller glia-derived
151 progenitors. We show that *mmp-9* is expressed in Müller glia, as they prepare to enter the cell
152 cycle, and Müller glia-derived progenitors. Using a loss-of-function mutant, we determine that

153 Mmp-9 negatively regulates the proliferation of Müller glia-derived progenitors. Finally, we
154 demonstrate that following photoreceptor regeneration, Mmp-9 is required for the maturation
155 and survival of regenerated cone photoreceptors.
156

157 **MATERIALS AND METHODS**

158 **Animals**

159 Wild-type, AB strain zebrafish (*Danio rerio*; ZIRC, University of Oregon, Eugene, OR) were
160 propagated, maintained, and housed in recirculating habitats at 28.5°C and on a 14/10-h
161 light/dark cycle. Embryos were collected after natural spawns, incubated at 28.5°C and staged
162 by hours post fertilization (hpf). Adults were of either sex and used between 6 and12 months of
163 age. The transgenic reporter line, *Tg[gfap:EGFP]*^{mi2002}*,* was used to identify Müller glia in retinal
164 sections (Bernardos and Raymond, 2006). All experimental protocols were approved by the
165 University of Michigan's Institutional Animal Care and Use Committee (IACUC).

166 **Light Lesions**

167 To kill photoreceptors, fish were dark adapted, then exposed to high intensity light (ca. 100,000
168 lux) for 30 minutes, followed by exposure to constant light (ca. 30.000 lux) for 72 hours (Taylor
169 et al., 2015). After 72 hours fish were returned to the recirculating habitats and normal light/dark
170 cycle.

171 **Plastic sections**

172 Eye cups were fixed overnight at 4°C in 2% PFA/2% glutaraldehyde in 0.1M phosphate
173 buffer, then infiltrated and embedded in glycol methacrylate plastic resin (JB-4; Polysciences,
174 Inc., Warrington, PA). Sections were cut at 4-µm, mounted on glass slides and stained with
175 .13% methylene blue and .13% basic fuchsin (Lee's stain).

176 **Quantitative Real-Time PCR**

177 Total RNA was extracted from dissected whole retinas using TRIzol (Invitrogen, Carlsbad, CA).
178 Reverse transcription to cDNA was performed using 1 µg RNA (Qiagen QuantiTect Reverse
179 Transcription kit; Venlo, Netherlands), and each qPCR reaction was performed with 6 ng cDNA
180 and Bio-Rad IQ SYBR Green Supermix (Bio-Rad CFX384 Touch Real Time PCR Detection
181 System; Hercules, CA). Three independent biological replicates were collected at each time
182 point, and each replicate contained six homogenized retinas from three fish (18 retinas/time

183 point). Each biological replicate was run in triplicate. For each time point, average mRNA levels
184 were represented as Log2 fold change, calculated using the DDC_T method and normalized to
185 the housekeeping gene, *gpia*. Primers used for qPCR analyses are listed in Table 1.

186 **Dexamethasone treatment**

187 A previously described protocol was used that efficiently suppresses the immune system in
188 zebrafish (Kyritsis et al., 2012; see also Bollaerts et al., 2019). Briefly, fish were housed in
189 system water with 15 mg/L dexamethasone (Sigma-Aldrich, Corp, D1756) diluted in 0.1%
190 MetOH. Dexamethasone-containing and control solutions were changed daily, and fish were fed
191 brine shrimp every other day.

192 **Immunohistochemistry**

193 Larvae or dissected eyecups were fixed overnight at 4°C in 0.1M phosphate buffered 4%
194 paraformaldehyde, cryoprotected with 20% sucrose, and embedded in optical cutting
195 temperature (OCT) medium (Sakura Finetek USA, Torrance, CA). Immunohistochemistry (IHC)
196 was performed as previously described (Taylor et al., 2015). Briefly, 10-µm-thick sections were
197 collected such that the optic nerve head was included, and sections were mounted onto glass
198 slides. Sections were washed in phosphate buffer saline with 0.5% Triton-x (PBST) and
199 incubated with 20% heat-inactivated normal sheep serum in PBST for 2 hours (NSS; Sigma-
200 Aldrich, Corp.). Primary antibodies were applied overnight at 4°C. Sections were then washed
201 with PBST and incubated in secondary antibodies for 1 hour at room temperature. Prior to IHC
202 for BrdU, sections were immersed in 100°C sodium citrate buffer (10 mM sodium citrate, 0.05%
203 Tween 20, pH 6.0) for 30 minutes and cooled at room temperature for 20 minutes. Sections
204 were then subjected to IHC as described above.

205 Immunohistochemistry performed on whole retinas was conducted as described
206 previously (Nagashima et al., 2017). Prior to IHC, retinas were dissected from dark-adapted
207 animals, flattened with radial relaxing cuts, fixed at 4^0C overnight in 4% paraformaldehyde in
208 0.1M phosphate buffer with 5% sucrose. Retinas were then placed in boiling sodium citrate

209 buffer for 5 min and allowed to cool for 5 min. Retinas were incubated for 2 hours in 10% normal
210 goat serum, 1% Tween, 1% Triton X-100, 1% DMSO, in phosphate buffered saline with 0.1%
211 sodium azide. Primary and secondary antibody were diluted in 2% normal goat serum, 1%
212 Tween, 1% Triton X-100, 1% DMSO, in phosphate buffered saline with 0.1% sodium azide and
213 incubations were performed overnight at room temperature. After washing in phosphate
214 buffered saline with 1% Tween, 1% Triton X-100, 1% DMSO, retinas were mounted on glass
215 slides, photoreceptor side down, in ProLong Gold anti-fade reagent (Life Technologies Corp.,
216 Eugene, OR). Antibodies used in this study and their concentrations are listed in Table 2.

217 **Labeling dividing cells**

218 For embryos, dividing cells were labeled with EdU by soaking embryos for 20 min in 1.5 mM
219 EdU dissolved in embryo rearing solution containing 15% DMSO. EdU was visualized using the
220 Click-iT™ EdU imaging kit (Thermo Fisher Scientific, Waltham, MA) with Alex Fluor 555
221 according to the manufacturer's protocol. In adults, dividing cells were labeled with BrdU by
222 housing animals in system water containing 5 mM BrdU for 24 hours (Gramage et al., 2015).

223 ***In situ* Hybridization**

224 *In situ* hybridizations were performed as previously described (Luo et al., 2012). Digoxigenin
225 (DIG)-labeled riboprobes for *rhodopsin* and *pde6c* were generated from full-length cDNA clones
226 (Luo et al., 2012; Ochocinska and Hitchcock, 2007), whereas riboprobe for *mmp-9* was
227 generated by PCR amplification using primers containing the T3 or T7 promoter sequences
228 (David and Wedlich, 2001). *mmp-9* (F): 5'
229 <u>TAATACGACTCACTATAGGG</u>GATTCTTCTACTTCTGCCGGG 3' *mmp-9* (R): 5'
230 <u>AATTAACCCTCACTAAAGGG</u>CTTAATAAATTTGTAAACAAG 3'.
231 Briefly, 10-μm-thick sections were hybridized with riboprobes at 55°C, incubated with an
232 alkaline-phosphatase-conjugated anti-DIG antibody and visualized using Fast Red TR/Naphthol
233 AS-MX (SIGMA*FAST*) as the enzymatic substrate. When *in situ* hybridizations were combined
234 with BrdU IHC, sections were removed from the fast red solutions, rinsed and post-fixed in

235 buffered 4% paraformaldehyde for 10 minutes then processed for BrdU IHC as described
236 above.

237 **Production of custom antibodies**

238 Antibodies specific to zebrafish Mmp-9 were generated by Pocono Rabbit Farm & Laboratory
239 (PRF&L, Canadensis, PA) as previously described (Calinescu et al., 2009). A 24 amino acid C-
240 terminal peptide was used as the immunogen, CDIDGIQYLYGPRTGPEPTAPQPR; NCBI:
241 AY151254. Polyclonal antibodies were affinity purified and confirmed by ELISA (data not
242 shown). Western blots performed with retinal proteins using pre- and post-immune sera
243 confirmed the post-immune serum detected a 76 kDa band, the predicted size for Mmp-9.
244 Western blot analysis and known cleavage sites on pro-Mmp9 suggest these antibodies
245 recognize both the pro- and active forms of Mmp-9, which can be distinguished by slight
246 differences in their molecular weights (Vandooren et al., 2013a; see Results).

247 **Western Blot Analysis**

248 Protein samples were obtained from whole retinas homogenized in RIPA lysis buffer
249 (ThermoFisher Scienific) containing protease and phosphatase inhibitor cocktail (5872S; Cell
250 Signaling Technology, Danvers, MA, USA). Proteins were separated in a 12% Mini-PROTEAN
251 TGX Precast gel (BioRad) and transferred to a polyvinylidene difluoride (PVDF) membrane
252 (GenHunter Corp., Nashville, TN). To block non-specific staining, membranes were incubated in
253 5% nonfat dry milk in Tris buffered saline containing 0.3% Tween-20 (TBST) for 2 hours.
254 Membranes were incubated with the antibodies-containing solution overnight at 4°C. Blots were
255 then washed in TBST and incubated with horseradish peroxidase-conjugated secondary IgG
256 (1:1000) for 1 hour at room temperature. Antibody-bound protein was visualized using Pierce
257 ECL Western blotting substrate (32106; ThermoFisher Scienific, Waltham, MA). To visualize
258 loading controls, blots were also stained with antibodies against actin. Images were captured
259 using the Azure C500 (Azure Biosystems, Dublin, CA). Densitometry of protein bands was
260 performed using ImageJ software (https://imagej.nih.gov/ij/).

261 **Zymography**

262 Protein samples were prepared as described for the Western blot analyses. Proteins were
263 separated on 10% Zymogram Plus (Gelatin) Protein Gels, (ThermoFisher Scientific). Following
264 electrophoresis, proteins were renatured in 1X renaturing buffer (ThermoFisher Scientific) for 30
265 mins at room temperature, then incubated in 1X developing buffer (ThermoFisher Scientific)
266 overnight at 37º. Gels were rinsed in deionized water and stained with SimplyBlue SafeStain
267 (ThermoFisher Scientific). Gels were imaged with long-wave ultraviolet light using the Azure
268 C500 (Azure Biosystems; Dublin, CA). Active recombinant human MMP-9 (Calbiochem, San
269 Diego, CA) was used as a positive control. Densitometry of the digested bands was performed
270 using ImageJ software.

271 **CRISPR-Cas9 mediated targeted mutation of Mmp-9**

272 *mmp-9* mutants were generated according to previously described methods (Hwang et al.,
273 2013). ZiFiT software (available in the public domain at zifit.partners.org) was used to identify a
274 19bp sgRNA target sequence for *mmp-9* (GGCTGCTTCATGGCATCAA). Target sequence
275 Oligo1- TTGATGCCATGAAGCAGCC and Oligo2-AAACTTGATGCCATGAAGCAG were
276 annealed and subcloned into the pT7 gRNA vector (Addgene ID: 46759). The pCS2 nCas9n
277 vector (Addgene ID: 46929) was used for Cas9 synthesis. To produce RNAs, the
278 MEGAshortscript T7 kit (Ambion, Foster City, CA: AM1354) and mirVana miRNA Isolation kit
279 (Ambion: AM 1560) were used for the gRNA, whereas, mMesage mMACHINE SP6 kit (Ambion:
280 AM1340) and RNeasy mini Kit from (Qiagen: 74104) were used for the Cas9 mRNA. Single cell-
281 stage embryos were injected with a 2nL solution containing 100 pg/nl sgRNA and 150 pg/nl
282 Cas9 mRNA. Founders (F0) were outcrossed to AB wild-type fish. Mutations were identified
283 using screening primers (F: 5′- AAGTCTGCAACTACATATCAGC -3′, R: 5′-
284 GTACACACTGTAGATGCTGATAAG-3') that flanked the *mmp-9* sgRNA target site. Standard
285 protocols for PCR used Platinum Taq-HF polymerase (Invitrogen) with genomic DNA as the
286 template. The purified PCR product was subcloned into the pGEM-T Easy vector (Promega,

287 Madison, WI) for Sanger sequencing. Mutant and wild-type sequences were aligned using
288 pairwise blast (National Center for Biotechnology Information [NCBI], Bethesda, MD, USA).
289 Premature stop codons were identified by comparing predicted amino acid sequences for wild-
290 type and mutants using the ExPASy translate tool (available in the public domain at
291 (www.expasy.org). F1 hybrids carrying a *mmp-9* mutation were in-crossed and homozygous F2
292 mutants were identified by a combination of Sanger sequencing and T7 endonuclease assays
293 (New England Biolabs, Ipswich, MA) as previously described (www.crisprflydesign.org).

294 **Imaging**

295 Fluorescence images of retinal sections were captured using the Leica TCS SP5
296 confocal microscope (Leica Microsystems, Wetzlar, Germany). Cell counts were conducted
297 using z-stack images and analyzed with Imaris software (Bitplane, South Windsor, CT).
298 Regenerated photoreceptors were identified by the colocalization of DAPI, BrdU, and the ISH
299 markers *pde6c* (cones) or *rho* (rods).

300 **Cell Counts and area measurement.**

301 Cells were counted in both radial sections and retinal wholemounts. In radial sections,
302 cells were counted in three nonadjacent sections in each retina. The number of cells per retina
303 were averaged, and averages were computed for control and experimental groups. In
304 wholemounts stained with an antibody against the tight junction protein, ZO-1 (Nagashima et al.,
305 2017), cones were identified in optical sections taken at the outer limiting membrane as profiles
306 with perimeters greater than 3.5 μm. Cells were counted in five separate regions in each retina,
307 sampling a totaling 5625^2μm per retina. The average number of cells in control and
308 experimental groups were then averaged.

309 **Experimental Design and Statistical Analyses**

310 The statistical significance in mRNA levels between unlesioned and lesioned retinas was
311 calculated using an ANOVA (JMP 9.0; SAS Institute, Inc., Cary, NC). A p-value ≤ 0.05 was
312 considered significant. The statistical significance in the number of cells between control and

313 treated retinas was calculated using a student's *t*-test (GraphPad Prism Software, La Jolla, CA).
314 A *p*-value ≤ 0.05 was considered significant. Western and zymogram analyses consisted of
315 three independent biological replicates, and each replicate contained six homogenized retinas
316 from three fish (18 retinas per time point). Statistical significance between optical density values
317 of bands in control and experimental groups was calculated using an ANOVA (JMP 9.0, SAS
318 Institute, Inc., Cary, NC). A *p*-value ≤ 0.05 was considered significant.
319
320

321 **RESULTS**

322 **The expression of inflammatory genes is induced by photoreceptor ablation**

323 To characterize the inflammatory response during photoreceptor ablation and
324 regeneration, qPCR was used to quantify the expression of inflammatory genes, *mmp-9, tnf–α*,
325 *tnf-β, il-8, nfκb1,* and *nfκb2*, shown previously to regulate various forms of tissue regeneration in
326 zebrafish (de Oliveira et al., 2013; LeBert et al., 2015; Nelson et al., 2013; Karra et al., 2015).
327 The time course of gene expression follows closely the well-established time course for the
328 injury response in Müller glia and the appearance of the Müller glia-derived progenitors and their
329 subsequent differentiation into mature photoreceptors (Figure 1A; see (Gorsuch and Hyde,
330 2014)). Upregulation of gene expression can be detected by 8 hours post lesion (hpl), and the
331 rising phase in expression corresponds to the period when Müller glia prepare to enter the cell
332 cycle. Expression levels then slowly decline as the Müller glia-derived photoreceptor progenitors
333 divide, migrate to the outer nuclear layer and differentiate into regenerated photoreceptors (168
334 hpl; Figure 1A). Interestingly, among all the transcripts examined, *mmp-9* shows the greatest
335 change from the undamaged controls, peaking at 24-48 hpl. Further, by 168 hpl *mmp-9* levels
336 are reduced to only about 70% of the peak value (ANOVA F-ratio = 22.23, p= .0001; Figure 1A).
337 The pro-inflammatory cytokine, Tnf–α, has been posited to be responsible for initiating
338 photoreceptor regeneration in zebrafish (Gorsuch and Hyde, 2014; Nelson et al., 2013), but at
339 all time points in this assay, the levels of *tnf-α* expression were not significantly different from
340 controls. Our assay for *tnf-α* failed to replicate previous results (Nelson et al., 2013), and we
341 infer this is most likely a consequence of technical issues, perhaps reflecting differences
342 between the qPCR assay used here and the protein analysis used by Nelson et al. (2013).
343 Nonetheless, these data show that in zebrafish a photolytic lesion, which leads to photoreceptor
344 death, induces rapid expression of characteristic inflammatory genes that follows a time course
345 reflecting the well-described events that underlie photoreceptor regeneration. Further, the

346 expression of *mmp-9* remains significantly elevated as photoreceptor differentiation
347 commences.

348 **Inflammation regulates injury-induced proliferation and photoreceptor regeneration**

349 To determine if inflammation regulates aspects of photoreceptor regeneration, the
350 glucocorticoid steroid, dexamethasone (Dex), was used to suppress the inflammatory response.
351 A 14-day pre-lesion treatment with dexamethasone was chosen based on studies performed by
352 Kyritsis et al. (2012; see also White et al., 2017; Caldwell et al., 2019; Bollaerts et al., 2019),
353 and here the dose of dexamethasone, route of administration and sizes and ages of animals
354 were matched with Kyritis et al. (2012). Whereas this lengthy treatment with dexamethasone
355 may affect homeostatic function in all cells (Juszczak and Stankiewicz, 2018), this treatment in
356 the absence of a lesion does not directly alter constitutive proliferation or neurogenesis (Kyritsis
357 et al., 2012; White et al., 2017; Caldwell et al., 2019).

358 To validate the effectiveness of the Dex treatment, the expression levels of inflammatory
359 genes were quantified in control and Dex-treated groups. At 72 hpl, the expression of *mmp-9*, *il-*
360 *6*, and *nfκb1* were significantly decreased following dexamethasone treatment (p values =
361 .0001, .0061, .0003, respectively; Figure 1C). Dex treatment did not suppress the expression of
362 *tnf-α*, and there was marked variability in the qPCR results for *tnf-α*. The reasons for the failure
363 of the Dex treatment to suppress *il-8* expression are unresolved. Further, Dex suppression of
364 NFkB mediated gene transcription may directly or indirectly affect mmp9 expression and/or
365 activity.

366 Assays of cell proliferation and photoreceptor regeneration were performed for control
367 animals and animals treated with Dex. Dividing cells were labelled with BrdU between 24 and
368 48 hpl to mark progenitors that will give rise to regenerated photoreceptors (Figure 1B), and
369 regenerated photoreceptors were identified as BrdU-labeled nuclei surrounded by *in situ*
370 hybridization signal for either *rho* (rods) or *pde6c* (cones) at 7 dpl (Figure 2A). At 72 hpl, there

371 was significantly fewer BrdU-labeled cells in Dex-treated retinas compared to controls (p=
372 0.0079; Figure 1D, E). At 7 dpl, there were significantly fewer regenerated rod and cone
373 photoreceptors in Dex-treated groups compared to controls (Figure 2B, C; p=0.0012). These
374 results indicate that, consistent with data showing the requirement for inflammation in neuronal
375 regeneration in the forebrain of zebrafish (Kyritsis et al., 2012), inflammatory mechanisms also
376 promote photoreceptor regeneration in the retina.

377 **Müller glia and Müller glia-derived progenitors express *mmp-9***

378 MMP-9 belongs to a large family of Zn^{2}+-dependent proteases that target a variety of
379 substrates, such as extracellular matrix (ECM), growth factors, chemokines, and cytokines.
380 Mmp-9 serves diverse functions among vertebrates (Pedersen et al. 2015; Page-McCaw, et al.,
381 2007; Vandooren, 2013b; Iyer et al. 2012). Due to the varied roles played by *mmp-9* in
382 injured/regenerating tissues (Vandooren et al., 2014), and its persistent expression throughout
383 the time-course of photoreceptor regeneration (Figure 1A), the specific function of Mmp-9 was
384 investigated further. As a first step, *in situ* hybridization was performed to identify the cellular
385 patterns of expression of *mmp-9*. This was undertaken using the Müller glia reporter line,
386 *Tg[gfap:EGFP]mi2002* (Bernardos and Raymond, 2006), and BrdU labeling 24 hrs prior to
387 sacrifice. By *in situ* hybridization, *mmp-9* is not detectable in unlesioned retinas. In contrast, by
388 24 hpl, *mmp-9* is expressed exclusively in Müller glia, but at a time-point prior to their entry into
389 S-phase of the cell cycle (Figure 3A). By 48 hpl, ~97% of BrdU-labeled Müller glia express
390 *mmp-9* (Figure 3A, B). At 72 hpl, the expression of *mmp-9* decreases (Figure 3A, C), and the
391 cellular expression shifts to the Müller glia-derived progenitors, as evidenced by the absence of
392 eGFP in BrdU-labeled cells that express *mmp-9* (Figure 3A). These data indicated that
393 photoreceptor ablation induces the expression of *mmp-9* in Müller glia, and this expression
394 persists in Müller glia-derived progenitors. Further, these results suggest that *mmp-9* identifies
395 the subset of Müller glia that enter the cell cycle in response to a retinal injury.

396 **Mmp-9 protein is present and catalytically active following photoreceptor death**

397 In tissues, Mmp-9 is synthesized and secreted in a pro-form, as a zymogen, then
398 cleaved into an active protease, which can be distinguished by the slight difference in its
399 molecular weight (Chattopadhyay and Shubayev, 2009; Vandooren et al., 2013a). Western blot
400 analysis was used to characterize the induction of protein synthesis and cleavage, and
401 zymogram assays were used to determine the time course of protein synthesis and catalytic
402 activity for Mmp-9 during photoreceptor regeneration (Vandooren et al., 2013a, 2013b). By
403 these assays, Mmp-9 is not detectable in unlesioned retinas, consistent with the *in situ*
404 hybridization data (Figure 3A, 4A). At 16hpl, the first time point sampled, the un-cleaved, pro-
405 form of Mmp-9 is detected as an upper band in Western blots (Figure 4A). Mmp-9 levels peak
406 by 24hpl, and both forms of Mmp-9 are detected. Mmp-9 levels decrease between 24 and
407 72hpl, and during this interval the protein mostly appears in a slightly lower band, consistent
408 with the active form of the protein. Mmp-9 levels are undetectable by Western blot analysis at
409 5dpl (ANOVA F-ratio = 8.377, p =.0013) (Figure 4 A, B).
410 Mmp-9 was previously named gelatinase B because its substrate, shared with Mmp-2, is
411 denatured type-1 collagen (gelatin). In zymography, the polyacrylamide gel contains gelatin, and
412 after protein renaturation and gelatin staining, areas of protease activity appear as clear,
413 negatively-stained bands against the stained background (Chattopadhyay and Shubayev, 2009;
414 Vandooren et al., 2013a). To evaluate the catalytic activity of Mmp-9, the same protein samples
415 used for the Western blot analysis were used for zymography. Recombinant, active human
416 MMP-9 was used as a positive control and shows strong catalytic activity as evidenced by the
417 large negatively-stained band. Unlesioned retinas contain no detectable Mmp-9 catalytic
418 activity. In contrast, the catalytic activity parallels the data from the Western blot analysis
419 (ANOVA F-ratio = 11.870, p = .0003) (Figure 4C, D). Together, results from the Western blot
420 and zymogram analyses show that catalytically-active Mmp-9 is induced by a lesion that
421 selectively injures photoreceptors, and the time course of Mmp-9 synthesis and catalytic activity
422 parallels the proliferative phases of photoreceptor regeneration.

423 **CRISPR mutants lack Mmp-9 protein and catalytic activity**

424 To investigate the function of *mmp-9* during photoreceptor regeneration, mutants were
425 generated using CRISPR-Cas9 (Hwang et al., 2013), targeted to the *mmp-9* catalytic domain in
426 exon 2 (Figure 5A). The 19 base sgRNA produced several alleles, two of which were bred to
427 homozygosity and characterized further, a 23bp deletion (designated *mi5003*; ZFIN,
428 https://zfin.org/) and an 8bp insertion (designated *mi5004*; ZFIN, https://zfin.org/), respectively
429 (Figure 5B). Individuals from the two lines were crossed to create compound heterozygotes to
430 evaluate the potential for off target effects in either of the two independent lines (see next
431 section). Each of the two *mmp-9* lines carries a mutation that results in a frameshift that predicts
432 premature stop codons (Extended Data supporting Figure 5 labeled as Figure 5-1). Retinas
433 from mutants were characterized by Western blot analysis and zymography. Unlesioned retinas
434 had no detectable Mmp-9 or catalytic activity (Figure 5C, D). As expected, following
435 photoreceptor ablation, Mmp-9 protein and catalytic activity are present in wild-type retinas
436 (Figure 5C, D). In contrast, there was trace Mmp-9 and catalytic activity in the *mi5004* line, but
437 no detectable Mmp-9 or catalytic activity in *mi5003* line (Figure 5C, D). Based on these results,
438 subsequent regeneration experiments were conducting using the *mi5003* line, though the basic
439 observations reported here were confirmed in the *mi5004* line (data not shown) and the
440 compound heterozygotes (see below).

441 **In Mmp9 mutants, photoreceptor death results in overproduction of photoreceptor**
442 **progenitors and regenerated photoreceptors**

443 We first sought to determine if there were any differences in retinal development or adult
444 starting points for the injury-induced proliferation in the *mmp-9* mutants. At 72 hpf, there were no
445 differences between wildtype and the two mutant lines in the size of the eyes or degree of
446 proliferation (Figure 6A, B, C), indicating early retinal development was not altered by the
447 absence of Mmp9. Similarly, qualitative comparisons of adult retinas showed the appearance of
448 wildtype and mutant retinas did not vary in any identifiable manner (Figure 7A). Finally,

449 comparing the number of Müller glia and the number of mitotic progenitors, which support
450 persistent neurogenesis in adult retinas (Raymond et al., 2006), showed there were no
451 quantitative differences between wild-type animals and the *mi5003* line in the number of Müller
452 glia or the level of intrinsic cell proliferation (Figure 7B,C).

453 To determine the consequence of Mmp-9 loss-of-function on retinal regeneration, wild-
454 type and mutant animals received photolytic lesions, Müller glia-derived progenitors were
455 labeled with BrdU between 48-72hpl, and BrdU-labeled cells were counted at 72 hpl. Relative to
456 wild-type animals, mutants had significantly more BrdU-labeled progenitors at 72 hpl ($p = .0186$)
457 (Figure 8A, B). This over production of the Müller glia-derived progenitors was observed in both
458 mutant lines and compound heterozygotes (Figure 7C), indicating that the hyperproliferation
459 observed here is unlikely to be a consequence of off-target effects induced by the CRISPR-cas9
460 technique.

461 It is well established that Mmp-9 plays a role in tissue remodeling and cell migration
462 (Parks et al., 2004). No overt tissue remodeling was observed following photoreceptor death
463 and during photoreceptor regeneration. To determine if Mmp-9 loss-of-function alters the
464 migration of Müller glia-derived progenitors from the inner nuclear layer, where Müller glia
465 reside, to the outer nuclear layer, which contains the photoreceptor nuclei, animals were
466 subjected to photolytic lesions, exposed to BrdU between 48 and 72hpl and allowed to survive
467 to 7dpl, a time point where proliferation and migration are complete and photoreceptor
468 differentiation has commenced. Qualitative inspection shows that Mmp-9 loss-of-function does
469 not alter the migration of the Müller glia-derived progenitors (Figure 8C). Further, cell counts
470 show that the over production of photoreceptor progenitors observed in mutants at 72hpl results
471 in significantly more BrdU-labeled cells within the ONL at 7dpl ($p = .0001$; Figure 9B, D).
472 Further, at 7 dpl, there are significantly more regenerated rod and cone photoreceptors ($p =$
473 $.0301$ and $p = .0005$, respectively; Figure 8E-G). Together, these data show that, in the absence
474 of an injury, Mmp-9 loss-of-function has no impact retinal development, the proliferative

475 potential of the adult retina or, following photoreceptor death, the migration of Müller glia-derived
476 progenitors. The hyperproliferation of injury-induced progenitors in mutants indicates that Mmp-
477 9 functions as a negative regulator of proliferation among Müller glia-derived progenitors,
478 though the mechanistic details through which this is accomplished are not yet known (see
479 Discussion). Further, the parallel overproduction of photoreceptors at 7dpl indicates that Mmp-9
480 plays no apparent role in governing the timing of cell cycle exit or the onset of photoreceptor
481 differentiation.

482 **Mmp-9 governs maturation and survival of regenerated cone photoreceptors**

483 The qPCR data showed that *mmp-9* levels remain significantly elevated at the time
484 injury-induced photoreceptor progenitors exit the cell cycle and begin differentiating into mature
485 photoreceptors (Figure 1A). We infer that, though not detected by Western blot analysis, Mmp-9
486 protein persists as well. This suggests that Mmp-9 may have functional roles beyond regulating
487 proliferation during the initial stages of photoreceptor regeneration. Therefore, regenerated rod
488 and cone photoreceptors were qualitatively and quantitatively compared in wild-type and
489 mutants at 21dpl, a time point where regeneration is complete (Powell et al., 2016). For both
490 groups, retinal sections were labeled with rod- and cone-specific antibodies and regenerated
491 photoreceptors were counted in sections and whole mount preparations. These analyses
492 showed there were no qualitative differences between wild-type and mutants in the appearance
493 of regenerated rod photoreceptors (Figure 9A), and the over production of rod photoreceptors
494 observed at 7dpl was present at 21dpl (Figure 9B, C).

495 In mutant retinas at 21dpl, the maturation and survival of cones were clearly
496 compromised. Relative to controls, regenerated cones in mutants have shorter outer segments
497 and appear to be fewer in number (Figure 9A, insets 9B,C). Counts of regenerated cones in
498 tissues sections show the initial over production of cones, evident at 7 dpl, is absent at 21 dpl
499 (Figure 9C). Cones were also counted in retinal wholemounts (Figure 10). In both wild-type and
500 mutant retinas, cone photoreceptors in unlesioned retinas are characterized by a very precise

501 lattice mosaic, a feature of cone photoreceptors in teleost fish (Nagashima et al., 2017; Figure
502 10A). The number of cone photoreceptors in unlesioned retinas from wild type and the mutant
503 retinas were invariant (Figure 10B). Following photoreceptor ablation and regeneration, areas of
504 the retina that contain regenerated photoreceptors are identifiable by the marked spatial
505 degradation of the mosaic, though individual cone photoreceptors remain readily identifiable
506 (Nagashima et al., 2017). Counts of regenerated cones in wholemounts show that mutants have
507 significantly fewer regenerated cones than wildtype animals (p=.0229) (Figure 10A, B). Finally,
508 as an independent measure of the maturation of cone photoreceptors, Western blot analysis
509 was performed using an antibody against the cone-specific transducin protein, Gnat-2 (Figure
510 10C; Lagman et al., 2015). As suggested by the invariant number of cones in unlesioned
511 retinas, Gnat-2 levels in unlesioned retinas are comparable in wild-type and mutant animals. In
512 lesioned retinas, Gnat-2 levels begin to recover in wild-type animals by 14 dpl, and by 21 dpl
513 values in wild-type animals are nearly at the levels found in unlesioned retinas (Figure 10C, D).
514 In contrast, Gnat-2 levels in mutants lag behind wild-type levels, and at 21dpl Gnat-2 levels in
515 mutant animals are significantly less than in wild-types (p = .0014) (Figure 10C, D). Comparable
516 measures specific to rod photoreceptors showed there were no differences between wild-type
517 and mutant animals (data not shown). These results indicate that Mmp-9 also plays a functional
518 role during photoreceptor regeneration, well after injury-induced proliferation and the initial
519 differentiation of regenerated photoreceptors is complete. Further, this function is specific to
520 cones.

521 **Late anti-inflammatory treatment rescues the maturation and survival defect of**
522 **regenerated cones in *mmp-9* mutants**

523 MMP-9 is known to cleave inflammatory cytokines, and we hypothesize it may function
524 to modify cytokine signaling during the resolution phase of tissue inflammation. To determine if
525 the defects in the maturation and survival of cone photoreceptors is a consequence of persistent
526 inflammation, we treated mutants with vehicle or Dex between 3 and 13dpl to suppress the

527 inflammatory response, beginning after the initial formation of Müller glia-derived progenitors
528 and throughout the phase of photoreceptor differentiation and maturation (Figure 11A). Cone
529 photoreceptors were then counted in retinal wholemounts at 21dpl from vehicle and Dex-treated
530 mutants. The number of cones at 21dpl in vehicle-treated mutants approximates that shown
531 above (Figure 10B; Figure 11mB, C). In contrast, there were significantly more regenerated
532 cones in the Dex-treated mutants than in the vehicle-treated controls (Figure 11B, C; p =.01),
533 restoring the number of regenerated cones nearly to that observed in wild-type animals. Further,
534 regenerated cones in the Dex-treated mutants were noticeably more mature than in controls, as
535 evidenced by their more regular arrangement and increased overall length (Figure 11D).
536 Correlated with these data, activated microglia are present in the ONL of vehicle-treated
537 mutants (Figure 11E), a notable feature of the early stages of photoreceptor death and a
538 hallmark of inflammation in the retina (White et al., 2017). These results suggest that the
539 absence of Mmp-9 results in a persistent immune activation, which selectively compromises the
540 survival and maturation of cone photoreceptors.
541

542 **DISCUSSION**

543 The results of this study are summarized in Figure 13. In response to photoreceptor cell
544 death, Müller glia undergo a single asymmetric division through interkinetic nuclear migration to
545 produce progenitors, which rapidly proliferate, migrate and differentiate to replace the ablated
546 photoreceptors (Figure 13A, B). Dexamethasone-induced immunosuppression inhibits
547 proliferation, resulting in diminished photoreceptor regeneration (Figure 13C). Loss of Mmp-9
548 function effectively reverses the consequences of immunosuppression, resulting in
549 hyperproliferation and overproduction of regenerated photoreceptors (Figure 13D). However,
550 the absence of Mmp-9 leads to defects in the survival and maturation of cone photoreceptors
551 (Figure 13D). Immunosuppression in mutants following photoreceptor regeneration rescues the
552 maturation and survival defects (Figure 13E). Based on these results, we conclude that
553 inflammation is required during the proliferative phase of photoreceptor regeneration, and as a
554 component of the inflammatory response, Mmp-9 provides an inhibitory balance that refines this
555 proliferative response. Finally, we conclude that Mmp-9 is required for the survival and
556 maturation of regenerated cone photoreceptors.

557 Immune system activation is required for regenerative neurogenesis (Fischer et al.,
558 2014; Kyritsis et al., 2012; White et al., 2017; Caldwell et al., 2019). In the forebrain and
559 brainstem of adult zebrafish, immunosuppression inhibits the production of progenitors after
560 traumatic lesion (Kyritsis et al., 2012; Caldwell et al., 2019). In the retina of larval zebrafish,
561 immunosuppression results in decreased migration of microglia into the outer retina during the
562 regeneration of rod photoreceptors (White et al., 2017). In the chick, ablation of microglia
563 completely suppresses the formation of Müller glia-derived retinal progenitors (Fischer et al.,
564 2014). Our data are consistent with these reports and indicate that acute inflammation is a
565 required component of neuronal regeneration in the vertebrate central nervous system.

566 Based on their structure and specific substrates, MMPs are classified into six groups:
567 gelatinases, collagenases, MTMMPs, stromelysins, and matrilysins (Vandooren, et al., 2013b).

568 MMP-9 is a secreted protease that is a member of the gelatinases. In response to photoreceptor
569 injury and death, *mmp-9* is rapidly induced in Müller glia, and anti-inflammatory treatment
570 significantly suppresses *mmp-9* expression. These data suggest Mmp-9 as a component of the
571 inflammatory response in the retina. Several previous reports showed that following neuronal
572 death Müller glia secrete the inflammatory cytokines, *tnf-α*, *leptin*, and *il-6* (Nelson et al., 2013;
573 Zhao et al., 2014). Recent transcriptome and gene ontology analysis for Müller glia, isolated
574 during photoreceptor injury and death, identified cytokine signaling and the immune response as
575 activated pathways (Roesch et al., 2012; Sifuentes et al., 2016). However, in the mammalian
576 retina, neuronal death leads to persistent active gliosis in Müller glia and failure of the
577 spontaneous expression of intrinsic reprogramming factors. This limits the ability for neuronal
578 regeneration (Bringmann et al., 2006, 2009; Reichenbach and Bringmann, 2013; see also Ueki
579 et al., 2015). Our data add details to the innate immune response in the retina that is required
580 for stem cell-based regeneration of photoreceptors. It is interesting to note that the activation of
581 cytokine pathways is conserved in the transcriptomes of Müller glia in both zebrafish and mouse
582 models of photoreceptor degeneration (Roesch et al., 2012; Sifuentes et al., 2016), suggesting
583 that photoreceptor death in vertebrates results in a common inflammatory response among
584 Müller glia.

585 Mmp-9 loss-of-function results in an increased number of Müller glia-derived progenitors,
586 resulting initially in more regenerated photoreceptors. The overproduction of regenerated
587 photoreceptors is interpreted simply to result from the overproduction of progenitors, and Mmp-9
588 plays no role in the timing of cell cycle exit or initial photoreceptor differentiation. There are at
589 least three interpretations that explain the overproduction of photoreceptor progenitors. First, the
590 absence of Mmp-9 may allow more Müller glia to enter the cell cycle. Previous studies showed
591 that neuronal damage results in only 65-75% of the Müller glia entering the cell cycle
592 (Nagashima et al., 2013). However, we demonstrated that *mmp-9* was expressed only by
593 dividing Müller glia. The absence of proliferation in *mmp-9*-negative Müller glia argues against

594 the possibility that additional Müller glia are recruited to the cell cycle. Second, in the *mmp-9*
595 mutants Müller glia may undergo more than a one round of cell division, thereby increasing the
596 size of the initial pool of Müller glia-derived progenitors, which then divide at a normal rate. We
597 do not favor this possibility, given a single asymmetric division among Müller glia is a hallmark
598 of regenerative neurogenesis in the zebrafish retina. Third, in the *mmp-9* mutants, proliferation
599 of the Müller glia-derived progenitors is accelerated. We view this the likeliest of the three
600 possibilities, and hypothesize that, as an extracellular protease, Mmp-9 regulates the
601 concentration of cytokines and/or growth factors that regulate cell cycle kinetics within the niche
602 of progenitors that cluster around each parental Müller glia, and in the absence of Mmp-9,
603 mitogenic signals persist, leading to accelerated proliferation (Bosak et al., 2018; Le et al., 2007;
604 Manicone and Mcguire, 2008; Parks et al., 2004; Luo et al., 2012; Vandooren et al., 2013b)..
605 Finally, we speculate that in regenerating tissues the magnitude of the inflammatory response
606 serves to quantitatively match the number of injury-induced progenitors to the degree of the cell
607 death.

608 White et al, (2017) showed that in larval zebrafish the timing of immune suppression can
609 delay or accelerate the regeneration of rod photoreceptors. As a pre-treatment, dexamethasone
610 suppresses the regeneration of rods. This result aligns with what we report here for adults,
611 inflammatory events are required for the activation of Müller glia and Müller glia-derived
612 progenitors. However, if dexamethasone treatment commences after rod photoreceptor ablation
613 (White et al., 2017), regeneration kinetics are enhanced. The enhanced regeneration following
614 delayed immune suppression parallels the results from the Mmp-9 mutants, but it is unlikely a
615 common mechanism can readily account for both results. The molecular milieu is complex in
616 injured tissues, and the potential parallels between delayed suppression of inflammation and the
617 absence of Mmp-9 await further characterization.

618 Recently, Kaur et al (2018) demonstrated a regulatory feedback loop involving Shh
619 signaling and Mmp-9 during retinal regeneration in zebrafish. Pharmacological and genetic

620 suppression of Shh signaling inhibited the proliferative response of Müller glia and their
621 progenitors. This was accompanied by up-regulation of *mmp-9* and the repressor of
622 proliferation, *insm1a* (Kaur et al., 2018; Ramachandran et al., 2012). The hyperproliferation we
623 observed in the *mmp-9* mutants is consistent with their proposed model. When Shh signaling
624 declines, progenitors increase secreted Mmp-9, which then degrades extracellular factors that
625 facilitate proliferative competence, resulting in increased *insm1a* and exit from cell cycle. In this
626 model, the absence of Mmp-9 would fail to degrade factors that stimulate proliferation, leading
627 to hyperproliferation. The positive feedback loop between Shh signaling and Mmp-9 suggests
628 that Shh and HB-EGB, factors that function upstream of *insm1a*, may be proteolytic substrates
629 for the Mmp-9 (Wan et al., 2012).

630 An inconsistency in the Kauer et al., (2018) study is their observation that morpholino
631 inhibition of Mmp-9 action decreases the production of Müller glia-derived progenitors. This
632 report is inconsistent with our data from the *mmp-9* mutants and raises the possibility that (1)
633 the reliance on morpholinos, with the recognized potential for off-target effects (Schulte-Merker
634 and Stainier, 2014; Kok et al., 2015; Stanier et al., 2017), may be the origin of these inconsistent
635 data, or (2) their injury paradigm, which results in bloodborne factors and cells (White et al.,
636 2017) invading the retina, may result in the activation of signaling pathways not present in the
637 retina following a photolytic lesion.

638 In the Mmp-9 loss-of-function mutants, survival and maturation of regenerated cone
639 photoreceptors are compromised. It is well established that chronic inflammation is a risk factor
640 for photoreceptor dystrophies in humans, such as retinitis pigmentosa and age-related macular
641 degeneration (AMD; Kauppinen et al., 2016; Chen and Xu, 2012; Whitcup et al., 2013; Yoshida
642 et al., 2013). A subset of patients with AMD exhibit single nucleotide polymorphism (SNP)
643 variants in the *MMP-9* gene, and elevated inflammation is associated with AMD pathogenesis
644 (Fritsche et al., 2016; Kauppinen et al., 2016; Parks et al., 2004). Mutational variants in the
645 inflammatory regulators, TIMP-3, TGFB, TNF-α are also identified in human patients with AMD

646 (Fritsche et al., 2016). We hypothesize that during photoreceptor regeneration in zebrafish,
647 Mmp-9 functions late to resolve the acute inflammation stimulated by death of the
648 photoreceptors, and, in the *mmp-9* mutants, there is prolonged inflammation that is selectively
649 damaging to cones. The *mmp-9* mutants studied here may recapitulate elements of the
650 pathologies that are characteristic of inflammatory photoreceptor diseases in humans, including
651 AMD. Our study begins to shed light on the functional roles of Mmp-9 in the retina and a
652 potentially important link between intrinsic retinal immunity, human photoreceptor dystrophies
653 and photoreceptor regeneration.
654
655

656 **References**

657 Amor S, Puentes F, Baker D, van der Valk P. 2010. Inflammation in neurodegenerative
658 diseases. *Immunology* 129:154–169.
659 Ando K, Shibata E, Hans S, Brand M, Kawakami A. 2017. Osteoblast Production by Reserved
660 Progenitor Cells in Zebrafish Bone Regeneration and Maintenance. *Dev Cell* 43:643–
661 650.e3.
662 Bernardos RL, Barthel LK, Meyers JR, Raymond PA. 2007. Late-stage neuronal progenitors in
663 the retina are radial Müller glia that function as retinal stem cells. *J Neurosci* 27:7028–7040.
664 Bernardos RL, Raymond PA. 2006. GFAP transgenic zebrafish. *Gene Expr Patterns* 6:1007–
665 1013.
666 Bollaerts I, Van Houcke J, Beckers A, Lemmens K, Vanhunsel S, De Groef L, Moons L. 2019.
667 Prior Exposure to Immunosuppressors Sensitizes Retinal Microglia and Accelerates Optic Nerve
668 Regeneration in Zebrafish. *Mediators Inflamm*. Article ID:6135795.
669 Bonnans C, Chou J, Werb Z. 2014. Remodelling the extracellular matrix in development and
670 disease. *Nat Rev Mol Cell Biol* 15:786–801.
671 Borsini A, Zunszain PA, Thuret S, Pariante CM. 2015. The role of inflammatory cytokines as key
672 modulators of neurogenesis. *Trends Neurosci* 38:145–157.
673 Bosak V, Murata K, Bludau O, Brand M. 2018. Role of the immune response in initiating central
674 nervous system regeneration in vertebrates: learning from the fish. *Int J Dev Biol* 62:403–
675 417.
676 Bringmann A, Pannicke T, Grosche J, Francke M, Wiedemann P, Skatchkov SN, Osborne NN,
677 Reichenbach A. 2006. Müller cells in the healthy and diseased retina. *Prog Retin Eye Res*
678 25:397–424.
679 Bringmann A, Iandiev I, Pannicke T, Wurm A, Hollborn M, Wiedemann P, Osborne NN,
680 Reichenbach A. 2009. Cellular signaling and factors involved in Müller cell gliosis:
681 neuroprotective and detrimental effects. *Prog Retin Eye Res* 28:423–451.
682 Caldwell LJ, Davies NO, Cavone L, Mysiak KS, Semenova SA, Panula P, Armstrong JD, Becker
683 CG, Becker T. 2019. Regeneration of dopaminergic neurons in adult zebrafish depends on
684 immune system activation and differs for distinct populations. *J Neurosci.,* 8
685 Calinescu A-A, Raymond PA, Hitchcock PF. 2009. Midkine expression is regulated by the
686 circadian clock in the retina of the zebrafish. *Vis Neurosci* 26:495–501.
687 Chattopadhyay S, Shubayev VI. 2009. MMP-9 controls Schwann cell proliferation and
688 phenotypic remodeling via IGF-1 and ErbB receptor-mediated activation of MEK/ERK
689 pathway. *Glia* 57:1316–1325.
690 Chen M, Xu H. 2012. Inflammation in Age-Related Macular Degeneration – Implications for
691 Therapy, Inflammatory Diseases - Immunopathology, Clinical and Pharmacological Bases
692 (Mahin Khatami, ed), pp. 129-150. IntechOpen, DOI: 10.5772/25658.
693 David R, Wedlich D. 2001. PCR-based RNA probes: a quick and sensitive method to improve
694 whole mount embryo in situ hybridizations. Biotechniques 30:769–72, 74.
695 de Oliveira S, Reyes-Aldasoro CC, Candel S, Renshaw SA, Mulero V, Calado A. 2013. Cxcl8
696 (IL-8) mediates neutrophil recruitment and behavior in the zebrafish inflammatory response.
697 *J Immunol* 190:4349–4359.
698 Deverman BE, Patterson PH. 2009. Cytokines and CNS Development. *Neuron* 64:61–78.
699 Ekdahl CT, Kokaia Z, Lindvall O. 2009. Brain inflammation and adult neurogenesis: the dual role
700 of microglia. *Neuroscience* 158:1021–1029.
701 Fausett BV, Goldman D. 2006. A role for alpha1 tubulin-expressing Müller glia in regeneration of
702 the injured zebrafish retina. *J Neurosci* 26:6303–6313.
703 Fimbel SM, Montgomery JE, Burket CT, Hyde DR. 2007. Regeneration of inner retinal neurons
704 after intravitreal injection of ouabain in zebrafish. J Neurosci. 14:1712-24.

705 Fischer AJ, Zelinka C, Gallina D, Scott MA, Todd L. 2014. Reactive microglia and macrophage
706 facilitate the formation of Müller glia-derived retinal progenitors. *Glia* 62:1608–1628.
707 Fritsche LG, Igl W, Bailey JNC, Grassmann F, Sengupta S, Bragg-Gresham JL, Burdon KP,
708 Hebbring SJ, Wen C, Gorski M, Kim IK, Cho D, Zack D, Souied E, Scholl HPN, Bala E, Lee
709 KE, Hunter DJ, Sardell RJ, Mitchell P, Merriam JE, Cipriani V, Hoffman JD, Schick T,
710 Lechanteur YTE, Guymer RH, Johnson MP, Jiang Y, Stanton CM, Buitendijk GHS, Zhan X,
711 Kwong AM, Boleda A, Brooks M, Gieser L, Ratnapriya R, Branham KE, Foerster JR,
712 Heckenlively JR, Othman MI, Vote BJ, Liang HH, Souzeau E, McAllister IL, Isaacs T, Hall J,
713 Lake S, Mackey DA, Constable IJ, Craig JE, Kitchner TE, Yang Z, Su Z, Luo H, Chen D,
714 Ouyang H, Flagg K, Lin D, Mao G, Ferreyra H, Stark K, von Strachwitz CN, Wolf A, Brandl
715 C, Rudolph G, Olden M, Morrison MA, Morgan DJ, Schu M, Ahn J, Silvestri G, Tsironi EE,
716 Park KH, Farrer LA, Orlin A, Brucker A, Li M, Curcio CA, Mohand-Saïd S, Sahel J-A, Audo
717 I, Benchaboune M, Cree AJ, Rennie CA, Goverdhan SV, Grunin M, Hagbi-Levi S,
718 Campochiaro P, Katsanis N, Holz FG, Blond F, Blanché H, Deleuze J-F, Igo RP Jr, Truitt B,
719 Peachey NS, Meuer SM, Myers CE, Moore EL, Klein R, Hauser MA, Postel EA, Courtenay
720 MD, Schwartz SG, Kovach JL, Scott WK, Liew G, Tan AG, Gopinath B, Merriam JC, Smith
721 RT, Khan JC, Shahid H, Moore AT, McGrath JA, Laux R, Brantley MA Jr, Agarwal A, Ersoy
722 L, Caramoy A, Langmann T, Saksens NTM, de Jong EK, Hoyng CB, Cain MS, Richardson
723 AJ, Martin TM, Blangero J, Weeks DE, Dhillon B, van Duijn CM, Doheny KF, Romm J,
724 Klaver CCW, Hayward C, Gorin MB, Klein ML, Baird PN, den Hollander AI, Fauser S, Yates
725 JRW, Allikmets R, Wang JJ, Schaumberg DA, Klein BEK, Hagstrom SA, Chowers I, Lotery
726 AJ, Léveillard T, Zhang K, Brilliant MH, Hewitt AW, Swaroop A, Chew EY, Pericak-Vance
727 MA, DeAngelis M, Stambolian D, Haines JL, Iyengar SK, Weber BHF, Abecasis GR, Heid
728 IM. 2016. A large genome-wide association study of age-related macular degeneration
729 highlights contributions of rare and common variants. *Nat Genet* 48:134–143.
730 Gemberling M, Bailey TJ, Hyde DR, Poss KD. 2013. The zebrafish as a model for complex
731 tissue regeneration. *Trends Genet* 29:611–620.
732 Goldman D. 2014. Müller glial cell reprogramming and retina regeneration. *Nat Rev Neurosci*
733 15:431–442.
734 Gorsuch RA, Hyde DR. 2014. Regulation of Müller glial dependent neuronal regeneration in the
735 damaged adult zebrafish retina. *Exp Eye Res* 123:131–140.
736 Gramage E, D'Cruz T, Taylor S, Thummel R, Hitchcock PF. 2015. Midkine-a Protein
737 Localization in the Developing and Adult Retina of the Zebrafish and Its Function During
738 Photoreceptor Regeneration. *PLoS One* 10:e0121789.
739 Hindi SM, Shin J, Ogura Y, Li H, Kumar A. 2013. Matrix Metalloproteinase-9 Inhibition Improves
740 Proliferation and Engraftment of Myogenic Cells in Dystrophic Muscle of mdx Mice. *PLoS*
741 *One* 8:e72121.
742 Hwang WY, Fu Y, Reyon D, Maeder ML, Tsai SQ, Sander JD, Peterson RT, Yeh J-RJ, Keith
743 Joung J. 2013. Efficient genome editing in zebrafish using a CRISPR-Cas system. *Nat*
744 *Biotechnol* 31:227–229.
745 Hyatt GA, Schmitt EA, Fadool JM, Dowling JE. 1996.Retinoic acid alters photoreceptor
746 development in vivo. Proc Natl Acad Sci U S A. 93:13298-303.
747 Iyer RP, Nicolle LP, Gregg BF, Merry LL. 2012. The History of Matrix Metalloproteinases:
748 Milestones, Myths, and Misperceptions. *American Journal of Physiology*. 303: H919–30.
749 Juszczak GR, Stankiewicz AM. 2018. Glucocorticoids, genes and brain function. Prog
750 Neuropsychopharmacol Biol Psychiatry. 82:136-168.
751 Karra R, Knecht AK, Kikuchi K, Poss KD. 2015. Myocardial NF-κB activation is essential for
752 zebrafish heart regeneration. *Proc Natl Acad Sci U S A* 112:13255–13260.
753 Kauppinen A, Paterno JJ, Blasiak J, Salminen A, Kaarniranta K. 2016. Inflammation and its role
754 in age-related macular degeneration. *Cell Mol Life Sci* 73:1765–1786.
755 Kaur S, Gupta S, Chaudhary M, Khursheed MA, Mitra S, Kurup AJ, Ramachandran R. 2018. let-

7 MicroRNA-Mediated Regulation of Shh Signaling and the Gene Regulatory Network Is Essential for Retina Regeneration. *Cell Rep* 23:1409–1423.
Kizil C, Kaslin J, Kroehne V, Brand M. 2012. Adult neurogenesis and brain regeneration in zebrafish. *Dev Neurobiol* 72:429–461.
Kizil C, Kyritsis N, Brand M. 2015. Effects of inflammation on stem cells: together they strive? *EMBO Rep* 16:416–426.
Kok FO, Shin M, Ni CW, Gupta A, Grosse AS, van Impel A, Kirchmaier BC, Peterson-Maduro J, Kourkoulis G, Male I, DeSantis DF, Sheppard-Tindell S, Ebarasi L, Betsholtz C, Schulte-Merker S, Wolfe SA, Lawson ND 2015. Reverse genetic screening revealspoor correlation between morpholino-induced and mutant phenotypes in zebrafish. Dev Cell 32:97–108.
Kyritsis N, Kizil C, Brand M. 2014. Neuroinflammation and central nervous system regeneration in vertebrates. *Trends Cell Biol* 24:128–135.
Kyritsis N, Kizil C, Zocher S, Kroehne V, Kaslin J, Freudenreich D, Iltzsche A, Brand M. 2012. Acute inflammation initiates the regenerative response in the adult zebrafish brain. *Science* 338:1353–1356.
Lagman D, Callado-Pérez A, Franzén IE, Larhammar D, Abalo XM. 2015. Transducin duplicates in the zebrafish **retina** and pineal complex: differential specialisation after the teleost tetraploidisation. PLoS One. 10:e0121330.
LeBert DC, Squirrell JM, Rindy J, Broadbridge E, Lui Y, Zakrzewska A, Eliceiri KW, Meijer AH, Huttenlocher A. 2015. Matrix metalloproteinase 9 modulates collagen matrices and wound repair. *Development* 142:2136–2146.
Lenkowski JR, Raymond PA. 2014. Müller glia: Stem cells for generation and regeneration of retinal neurons in teleost fish. *Prog Retin Eye Res* 40:94–123.
Le NTV, Xue M, Castelnoble LA, Jackson CJ. 2007. The dual personalities of matrix metalloproteinases in inflammation. *Front Biosci* 12:1475–1487.
Liddiard K, Rosas M, Davies LC, Jones SA, Taylor PR. 2011. Macrophage heterogeneity and acute inflammation. *Eur J Immunol* 41:2503–2508.
Luo J, Uribe RA, Hayton S, Calinescu A-A, Gross JM, Hitchcock PF. 2012. Midkine-A functions upstream of Id2a to regulate cell cycle kinetics in the developing vertebrate retina. *Neural Dev* 7:33.
Manicone A, Mcguire J. 2008. Matrix metalloproteinases as modulators of inflammation. *Semin Cell Dev Biol* 19:34–41.
Masure S, Proost P, Van Damme J, Opdenakker G. 1991. Purification and identification of 91-kDa neutrophil gelatinase. Release by the activating peptide interleukin-8. *Eur J Biochem* 198:391–398.
Nagase H, Visse R, Murphy G. 2006. Structure and Function of Matrix Metalloproteinases and TIMPs. *Cardiovascular Research* 69: 562–73.
Nagashima M, Barthel LK, Raymond PA. 2013. A self-renewing division of zebrafish Müller glial cells generates neuronal progenitors that require N-cadherin to regenerate retinal neurons. *Development* 140:4510–4521.
Nagashima M, Hadidjojo J, Barthel LK, Lubensky DK, Raymond PA. 2017. Anisotropic Müller glial scaffolding supports a multiplex lattice mosaic of photoreceptors in zebrafish retina. *Neural Dev* 12:20.
Nathan C. 2002. Points of control in inflammation. *Nature* 420:846–852.
Nelson CM, Gorsuch RA, Bailey TJ, Ackerman KM, Kassen SC, Hyde DR. 2012. Stat3 defines three populations of Müller glia and is required for initiating maximal müller glia proliferation in the regenerating zebrafish retina. *J Comp Neurol* 520:4294–4311.
Nelson CM, Ackerman KM, O'Hayer P, Bailey TJ, Gorsuch RA, Hyde DR. 2013. Tumor necrosis factor-alpha is produced by dying retinal neurons and is required for Muller glia proliferation during zebrafish retinal regeneration. *J Neurosci* 33:6524–6539.
Ochocinska MJ, Hitchcock PF. 2007. Dynamic expression of the basic helix-loop-helix

807 transcription factor neuroD in the rod and cone photoreceptor lineages in the retina of the
808 embryonic and larval zebrafish. *J Comp Neurol* 501:1–12.
809 Opdenakker G, Masure S, Proost P, Billiau A, van Damme J. 1991. Natural Human Monocyte
810 Gelatinase and Its Inhibitor. *FEBS Letters* 284: 73–78.
811 Page-McCaw A, Andrew JE, Zena W. 2007. "Matrix Metalloproteinases and the Regulation of
812 Tissue Remodelling." *Nature Reviews. Molecular Cell Biology* 8: 221–33.
813 Parks WC, Wilson CL, López-Boado YS. 2004. Matrix metalloproteinases as modulators of
814 inflammation and innate immunity. *Nat Rev Immunol* 4:617–629.
815 Pedersen ME, Tram TV, Sissel BR, Svein, OK. 2015. Matrix Metalloproteinases in Fish Biology
816 and Matrix Turnover. *J Int Soc Matrix Biol.* 44-46: 86–93.
817 Powell C, Cornblath E, Elsaeidi F, Wan J, Goldman D. 2016. Zebrafish Müller glia-derived
818 progenitors are multipotent, exhibit proliferative biases and regenerate excess neurons. *Sci*
819 *Rep* 6:24851.
820 Ramachandran R, Zhao X-F, Goldman D. 2012. Insm1a-mediated gene repression is essential
821 for the formation and differentiation of Müller glia-derived progenitors in the injured retina.
822 *Nat Cell Biol* 14:1013–1023.
823 Raymond PA, Barthel LK, Bernardos RL, Perkowski JJ. 2006. Molecular characterization of
824 retinal stem cells and their niches in adult zebrafish. *BMC Dev Biol* 6:36.
825 Reichenbach A, Bringmann A. 2013. New functions of Müller cells. *Glia* 61:651–678.
826 Roesch K, Stadler MB, Cepko CL. 2012. Gene expression changes within Müller glial cells in
827 retinitis pigmentosa. *Mol Vis* 18:1197–1214.
828 Schulte-Merker S, Stainier DYR. 2014. Out with the old, in with the new: Reassessing
829 morpholino knockdowns in light of genome editing technology. Development 141:3103–
830 3104.
831 Sherpa T, Fimbel SM, Mallory DE, Maaswinkel H, Spritzer SD, Sand JA, Li L, Hyde DR,
832 Stenkamp DL. 2008. Ganglion cell regeneration following whole-retina destruction
833 in zebrafish. Dev Neurobiol. 68:166-81.
834 Shubayev VI, Angert M, Dolkas J, Marie Campana W, Palenscar K, Myers RR. 2006. TNFα-
835 induced MMP-9 promotes macrophage recruitment into injured peripheral nerve. *Mol Cell*
836 *Neurosci* 31:407–415.
837 Sifuentes CJ, Kim J-W, Swaroop A, Raymond PA. 2016. Rapid, Dynamic Activation of Müller
838 Glial Stem Cell Responses in Zebrafish. *Invest Ophthalmol Vis Sci* 57:5148–5160.
839 Stainier DYR, Raz E, Lawson ND, Ekker SC, Burdine RD, Eisen JS, Ingham PW, Schulte-
840 Merker S, Yelon D, Weinstein BM, Mullins MC, Wilson SW, Ramakrishnan L, Amacher SL,
841 Neuhauss SCF, Meng A, Mochizuki N, Panula P, Moens CB. 2017. Guidelines for
842 morpholino use in zebrafish. PLoS Genet. 13(10):e1007000. doi: 10.1371
843 Taylor SM, Alvarez-Delfin K, Saade CJ, Thomas JL, Thummel R, Fadool JM, Hitchcock PF.
844 2015. The bHLH Transcription Factor NeuroD Governs Photoreceptor Genesis and
845 Regeneration Through Delta-Notch Signaling. *Invest Ophthalmol Vis Sci* 56:7496–7515.
846 Thomas JL, Ranski AH, Morgan GW, Thummel R. 2016. Reactive gliosis in the
847 adult zebrafish retina. *Exp Eye Res*. 143:98-109.
848 Ueki Y, Wilken MS, Cox, KE, Chipman L, Jorstad N, Sternhagen K, Simic M, Ullom K, Nakafuku
849 M, Reh TA. 2015. Transgenic expression of the proneural transcription factor Ascl1 in
850 Müller glia stimulates retinal regeneration in young mice. *Proc Nat Acad Sci* 112:13737-
851 13722.
852 Vandooren J, Geurts N, Martens E, Van den Steen PE, Opdenakker G. 2013a. Zymography
853 methods for visualizing hydrolytic enzymes. *Nat Methods* 10:211–220.
854 Vandooren J, Van den Steen PE, Opdenakker G. 2013b. Biochemistry and molecular biology of
855 gelatinase B or matrix metalloproteinase-9 (MMP-9): the next decade. *Crit Rev Biochem*
856 *Mol Biol* 48:222–272.
857 Vandooren J, Van Damme J, Opdenakker G. 2014. On the structure and functions of gelatinase

858 B/matrix metalloproteinase-9 in neuroinflammation. *Prog Brain Res* 214:193–206.
859 Vecil GG, Larsen PH, Corley SM, Herx LM, Besson A, Goodyer CG, Yong VW. 2000.
860 Interleukin-1 is a key regulator of matrix metalloproteinase-9 expression in human neurons
861 in culture and following mouse brain trauma in vivo. *J Neurosci Res* 61:212–224.
862 Wan J, Ramachandran R, Goldman D. 2012. HB-EGF is necessary and sufficient for Müller glia
863 dedifferentiation and retina regeneration. *Dev Cell* 22:334–347.
864 Whitcup SM, Nussenblatt RB, Lightman SL, Hollander DA. 2013. Inflammation in Retinal
865 Disease. *Int J Inflam* 2013:1–4.
866 White DT, Sengupta S, Saxena MT, Xu Q, Hanes J, Ding D, Ji H, Mumm JS. 2017.
867 Immunomodulation-accelerated neuronal regeneration following selective rod
868 photoreceptor cell ablation in the zebrafish retina. *Proc Nat Acad Sci* 114:E3719–E3728.
869 Xue Q, Cao L, Chen X-Y, Zhao J, Gao L, Li S-Z, Fei Z. 2017. High expression of MMP9 in
870 glioma affects cell proliferation and is associated with patient survival rates. *Oncol Lett*
871 13:1325–1330.
872 Xu S, Webb SE, Lau TCK, Cheng SH. 2018. Matrix metalloproteinases (MMPs) mediate
873 leukocyte recruitment during the inflammatory phase of zebrafish heart regeneration. *Sci*
874 *Rep* 8:7199.
875 Yoshida N, Ikeda Y, Notomi S, Ishikawa K, Murakami Y, Hisatomi T, Enaida H, Ishibashi T.
876 2013. Laboratory evidence of sustained chronic inflammatory reaction in retinitis
877 pigmentosa. *Ophthalmology* 120:e5–12.
878 Zhao X-F, Wan J, Powell C, Ramachandran R, Myers MG, Goldman D. 2014. Leptin and IL-6
879 Family Cytokines Synergize to Stimulate Müller Glia Reprogramming and Retina
880 Regeneration. *Cell Rep* 9:272–284.

881

882 **Figure Legends**
883
884 **Figure 1: Inflammation is induced following photoreceptor ablation and regulates**
885 **reactive-proliferation.**
886 **(A)** Time-course for the expression of inflammatory genes, from 8 to 168 hours post lesion (hpl).
887 Unlesioned retinas served as controls. Expression levels are represented as fold change
888 calculated using DDC_T method. **(B)** Experimental paradigm for anti-inflammatory treatment with
889 Dex and BrdU labeling. **(C)** qRT-PCR for the inflammatory genes *mmp-9, tnf-a, nfkb1, il-8,* and
890 *il-6* from control and Dex-treated retinas at 72 hpl. *p≤0.05. **(D)** BrdU immunostained cells
891 (green) in controls (left) and Dex-treated animals (right) at 72 hpl. **(E)** Number of BrdU-labeled
892 cells in controls (268 ± 36.1 cells; n=5) and Dex-treated animals (160.2 ± 20.02 cells; n=5) at 72
893 hpl; *p=0.0079. ONL- outer nuclear layer; INL- inner nuclear layer; GCL- ganglion cell layer.
894 Scale bar equals 50μm.
895
896 **Figure 2: Anti-inflammatory treatment suppresses photoreceptor regeneration.**
897 **(A)** Experimental paradigm of anti-inflammatory treatment. **(B)** Double labeled, regenerated
898 photoreceptors using *in situ* hybridization for rods (*rho) and cones (pde6c;* red signal) and BrdU
899 (green). The high magnification insets show the colocalization of the two labels (asterisks). **(C)**
900 Number of regenerated rod photoreceptors in control (29.52 ± 4.1 cells; n=7) and experimental
901 retinas (1833 ± 5.71 cells; n=7); *p=0.0047. **(D)** Number of regenerated cone photoreceptors in
902 control (42 ± 6.1 cells; n=7) and Dex-treated animals (25 ± 11.72 cells; n=7). *p=0.0012. ONL-
903 outer nuclear layer; INL- inner nuclear layer; GCL- ganglion cell layer. Scale bar equals 50μm.
904
905 **Figure 3: Following a photolytic lesion, Müller glia and Müller glia-derived progenitors**
906 **express *mmp-9*.**
907 These experiments were performed using the transgenic line *Tg[gfap:EGFP]mi2002*, in which
908 eGFP is expressed in Müller glia. **(A)** Triple labeling using *in situ* hybridization for *mmp-9* (red)
909 and immunostaining for BrdU for dividing cells (white), combined with GFP immunostaining
910 (green). **(B)** Number of BrdU+ cells that express *mmp-9* in unlesioned animals and lesioned
911 animals at 24, 48, and 72 hpl. **(C)** Number of GFP+ Müller glia that also express *mmp-9*
912 expression at 24, 48, and 72 hpl. ONL- outer nuclear layer; INL- inner nuclear layer; GCL-
913 ganglion cell layer. Scale bar equals 25μm.
914
915 **Figure 4: Mmp-9 is expressed and catalytically active following photoreceptor death.**
916 **(A)** Western blot of retinal proteins from unlesioned retinas (UL) and lesioned retinas at 16 hpl,
917 24 hpl, 48 hpl, 72 hpl, and 120 hpl, stained with anti-Mmp-9 and anti-actin (loading control)
918 antibodies. **(B)** Densitometry of Mmp-9 protein, plotted relative to unlesioned controls. **(C)**
919 Zymogram of Mmp-9 catalytic activity from unlesioned retinas (UL) and lesioned retinas at 16,
920 24, 48, 72 and 120hpl. Lanes in zymogram correspond to those in the Western blot. Purified
921 human recombinant protein serves as a positive control. **(D)** Densitometry of Mmp-9 catalytic
922 activity, plotted relative to the positive control.
923
924 **Figure 5: CRISPR mutants lack catalytically-active Mmp-9.**
925 **(A)** Genomic structure of *mmp-9* and the gRNA target sequence. **(B)** Sequence alignment for
926 two indel mutations - 8 bp insertion (*mmp-9*^{mi5004}) and 23 bp deletion (*mmp-9*^{mi5003}). Red
927 underline indicates the sequence targeted by the 19 bp gRNA. **(C)** Western blot of retinal
928 proteins from unlesioned retinas (UL wild-type; UL *mmp-9*^{mi5004}; UL *mmp-9*^{mi5003}) and lesioned
929 retinas (wild-type; *mmp-9*^{mi5004}; *mmp-9*^{mi5003}) at 16, 24, and 48 hpl immunostained with anti-
930 Mmp-9 and anti-actin (loading control) antibodies. **(D)** Zymogram of Mmp-9 catalytic activity.
931 Lanes in zymogram correspond to those in the Western blot. Purified human recombinant
932 protein serves as a positive control.

933
934
935 **Figure 6. Retinal development is unaltered by the absence of mmp-9**.
936 **(A)** Sections from 72 hpf larvae immunostained (arrowheads) for ganglion cells (ZN5), rod
937 photoreceptors (ZPR-3), and amacrine cells (HPC1). **(B)** Quantification of retinal area in wild-
938 type (722.36 ±105.39 µm; n=12) compared to mmp9 mutants (676.95 ± 75.05 µm; n=9), p=.286.
939 **(C)** Quantification of the area of EdU-labeled cells, as an indicator of proliferation, in wild-type
940 (30 ± 7.84µm; n=12) and to mmp9 mutants (33.5 ± 6.59 µm; n=9), p=.293. Scale bar equals 25
941 μm.
942
943 **Figure 7. Anatomy of adult retina in Mmp-9 mutants. (A)** Plastic sections illustrating cellular
944 and synaptic layers in adult retinas from wildtype and Mmp-9 mutants. These slightly oblique
945 sections also reveal elements of the cone photoreceptor mosaic. **(B)** Processes of Müller glia
946 (green) stained with the zrf-1 antibody (top). BrdU-labeled cells (red, indicated by arrowheads)
947 in wild-type and mutant retinas (bottom). **(B)** Immunostained Müller glia (top) and Brdu-labeled
948 cells (bottom) in wild-type and mutant retinas. **(C)** Number of Müller glia in wild-type (55.83 ±
949 1.23; n=4) and mutant retinas (54.58 ± 2.54; n=4), p=.409 and dividing cells (bottom) in wild-
950 type (3.66 ± 2.47; n=4) and mutant retinas (2.75 ± .92; n=4), p=.515. **(D)** BrdU-labeled cells
951 (red) in wild-type (left) and transheterozygote (TH) retinas, qualitatively illustrating the
952 overproduction of injury-induced progenitors in transheterozygotes. Scale bars equal 25μm.
953
954 **Figure 8: Photolytic lesions in *mmp-9* mutants results in the over production of injury-**
955 **induced progenitors and regenerated photoreceptors.**
956 **(A)** BrdU-labeled cells (green) in wild-type and *mmp-9* ^{mi5003}. **(B)** Number of BrdU+ cells from
957 wild-type (109 ± 19.66 cells; n=6) mutant retinas (142.3 ± 25.72 cells; n=9) at 72 hpl. *p =
958 0.0186. **(C)** BrdU-labeled cells (green) in wild-type and mutant retinas at 168 hpl. **(D)** Number of
959 BrdU+ cells in the ONL of wild-type (48 ± 10.24 cells; n=8) and mutant retinas (71.71 ± 3.7 cells;
960 n=8). *p=0.0001. **(E)** Double labeled, regenerated photoreceptors using *in situ* hybridization for
961 rods (*rho) and cones (pde6c;* red signal) and BrdU (green) at 168hpl. **(F)** Number of
962 regenerated cone photoreceptors in wild-type (31.42 ± 9.88 cell; n=8) and mutant retinas (43.83
963 ± 10.68 cells; n=8) at 168 hpl. *p=0.0301. **(G)** Number of regenerated rod photoreceptors in
964 wild-type (14.88 ± 4.02 cells; n=8) and mutant retinas (26.04 ± 5.69 cells; n=8) at 168 hpl.
965 *p=0.0005. . ONL- outer nuclear layer; INL- inner nuclear layer; GCL- ganglion cell layer. Scale
966 bars equal 50μm.
967
968 **Fig 9. Mmp-9 regulates the maturation of regenerated photoreceptors.**
969 **(A)** Immunostaining for red-green double cones with ZPR-1 and rods with ZPR-3. Wild-type are
970 in the top row; mutants are in the bottom row. Unlesioned retinas are left; lesioned retinas at21
971 dpl are right. **(B)** Double labeled, regenerated photoreceptors at 21dpl using *in situ* hybridization
972 for rods (*rho) and cones (pde6c;* red signal) and BrdU (green). Insets detail the morphology of
973 regenerated photoreceptors in wild-type (left) and mutant retinas (right). **(C)** Number of
974 regenerated cone photoreceptors (bottom) in wild-type (95.81 ± 18.49 cells; n=6) and mutant
975 retinas (71.89 ± 20.37 cells; n=6) at 21 dpl. p=0.059. Number of of regenerated rod
976 photoreceptors (top) in wild-type (29.6 ± 4.94 cells; n=6) and mutant retinas (53.39 ± 21.62
977 cells; n=6) at 21 dpl. *p=0.0270. ONL- outer nuclear layer; INL- inner nuclear layer; GCL-
978 ganglion cell layer. Scale bar equals 50μm.
979
980 **Fig 10. Mmp-9 is required for the survival of regenerated cone photoreceptors.**
981 **(A)** Wholemounts of wild-type (left) and mutant retinas (right) immunostained for ZO-1.
982 Unlesioned retinas are top; lesioned retinas at 21dpl are bottom. Asterisks indicate profiles of

983 cones. In mutants, gaps due to missing cones are replaced by the irregular apical processes of
984 Müller glia (dashed lines). **(B)** Number of unlesioned cones from wild-type (546.49 ± 55.69;
985 n=5) and *mmp-9* ^{mi5003} (565.33 ± 27.42; n=5) *p=.516; below the number of regenerated cones
986 from wild-type (599.11 ± 27.42 cones; n=5) and mutant retinas (436.09 ± 128.04 cones; n=5) at
987 21 dpl. *p=0.0238. **(C)** Western blot of retinas stained with antibodies against gnat-2 and actin
988 at 7, 14, and 21 dpl. **(D)** Densitometry of gnat-2 labeling in the Western blot. A significant
989 difference in gnat-2 levels were observed at 21 dpl. *p=.0014. Scale bar equals 10 μm.
990
991 **Fig 11. Anti-inflammatory treatment rescues the maturation and number of regenerated**
992 **cones in mutants at 21dpl.**
993 **(A)** Experimental paradigm for the photolytic lesions and Dexamethasone treatment. **(B)**
994 Wholemounts of mutant retinas immunostained for ZO-1. Control retina is left; Dex-treated
995 retina is right. **(C)** Number of regenerated cones in control (292.20 ± 158.11 cones; n=6) and
996 Dex-treated retinas (522.79 ± 82.55 cones; n=6) at 21 dpl. *p=0.0010. **(D)** Immunostaining with
997 ZPR-1 for red-green double cones in control (top) and Dex mutants (bottom) 21 dpl. Insets
998 illustrate differences in the maturation and lengths of the cone photoreceptors (dashed lines;
999 control, 22.1 ± 7.2μm, n=40 cells; Dex-treated, 29.7 ± 4.8μm, n=69 cells; p<.001) **(E)**
1000 Immunostaining for microglia using the 4C4 antibody in control (top) and Dex-treated retinas
1001 (bottom). Inserts illustrate ameboid (top) and ramified (bottom) microglia. Scale bars equal
1002 10μm in panel A and 40μm in panels D and E.
1003
1004 **Fig 12. Summary Diagram of cone regeneration (A)** Müller glia respond to photoreceptor
1005 death by expressing *mmp-9*, undergoing interkinetic nuclear migration and a single asymmetric
1006 cell division that gives rise to a neuronal progenitor. **(B)** In wild-type animals, neuronal
1007 progenitors form a neurogenic cluster around the Müller glia (3 dpl), migrate to the ONL, and
1008 differentiate into cone photoreceptors (7 dpl) that then mature (21 dpl). **(C)** Anti-inflammatory
1009 treatment results in fewer Müller gli-derived progenitors and fewer regenerated photoreceptors.
1010 **(D)** In the absence of Mmp-9, there is overproduction of Müller glia-derived progenitors and
1011 regenerating photoreceptors. However, at 21dpl, cone maturation and survival are
1012 compromised. **(E)** In the absence of Mmp-9, anti-inflammatory treatment rescues the maturation
1013 and survival of cone photoreceptors. ONL- outer nuclear layer; INL- inner nuclear layer; GCL-
1014 ganglion cell layer.
1015
1016
1017 **Figure 5-1. Extended Data supporting Figure 5.**
1018 **(A)** Amino acid sequence alignments for Mmp-9 in wild-type and *mmp-9*^{mi5003} and *mmp-9*^{mi5004}
1019 mutants. The red amino acids denote the target of the gRNA. Insertion or deletion introduced a
1020 frameshift resulting in alteration of the amino acid sequence (*mmp-9*^{mi5003}) or protein truncation
1021 (*mmp-9*^{mi5004}).
1022
1023

1024
1025
1026
1027 **Table 1: Primer Sequences**

Name	Sequence
gpia	F) 5'- TCCAAGGAAACAAGCCAAGC-3' R) 5'- TTCCACATCACACCCTGCAC-3'
mmp-9	F) 5'- TGATGTGCTTGGACCACGTAA-3' R) 5'- ACAGGAGCACCTTGCCTTTTC-3'
tnf-α	F) 5'- GCGCTTTTCTGAATCCTACG-3' R) 5'- TGCCCAGTCTGTCTCCTTCT-3'
tnf-β	F) 5'- CCTCAGACCACGGAAAAGT-3' R) 5'- GCCCTGTTGGAATGCCTGAT-3'
il-6	F) 5'- TCTTTCCCTCTTTTCCTCCTG -3' R) 5'- TCAACTTCTCCAGCGTGATG -3'
il-8	F) 5'- GTCGCTGCATTGAAACAGAA -3' R) 5'- AGGGGTCCAGACAGATCTCC-3'
nfκb1	F) 5'- ACCAGACTGTGAGCGTGAAG -3' R) 5'- CGCAAGTCCTACCCACAAGT -3'
nfκb2	F) 5'- CATATGTCCCACACAATCAAGAC-3' R) 5'- AGCCACCATAATGATCTGGAA -3'

1028
1029
1030
1031
1032
1033
1034
1035
1036
1037
1038
1039
1040
1041
1042
1043
1044
1045
1046
1047
1048
1049
1050
1051
1052
1053

1054 **Table 2: Antibody List**

Primary Antibodies	Company	Dilution
Mouse monoclonal anti-GFP	Milipore MAB3580	1:200
Mouse monoclonal anti-actin	Calbiochem	1:1000
Mouse Monoclonal anti-Zn5	ZIRC; zfin.org/ZDB-ATB-081002-19	1:200
Mouse Monoclonal anti-Zpr1 (anti-Arrestin-3)	ZIRC; zfin.org/ZDB-ATB-081002-43	1:200
Mouse Monoclonal anti-Zpr-3	ZIRC; zfin.org/ZDB-ATB-081002-45	1:200
Mouse anti-HPC1	ZIRC; zfin.org/ZDB-ATB 130225-1	1:200
Mouse anti-Zrf1	ZIRC; zfin.org/ZDB-ATB-081002-46	1:1000
Mouse Monoclonal ZO-1A-12	Innovative Research Cat# 33-9100, RRID:AB_87181	1:200
Mouse anti-BrdU	BD Biosciences Ca# 347580	1:100
Rat anti-BrdU	Abcam Cat# ab6326, RRID:AB_305426	1:200
Polyclonal anti-GNAT2	MBL Ca# PM075	1:1000
Mouse Monoclonal anti-1D1 (ZF Rhodoposin)	Hyatt et al., 1996 Gift from Dr. Jim Fadool (FSU)	1:1000
Mouse Monoclonal anti-4C4 (zebrafish microglia)	Raymond et al., 2006 Hitchcock Lab	1:200
Secondary Antibodies		
Alexa Fluor goat anti-mouse 488, 555, or 647	Invitrogen	1:500
Alexa Fluor goat anti-rabbit 488, 555, or 647	Invitrogen	1:500
Alexa Fluor goat anti-rat 488, 555, or 647	Invitrogen	1:500

1055

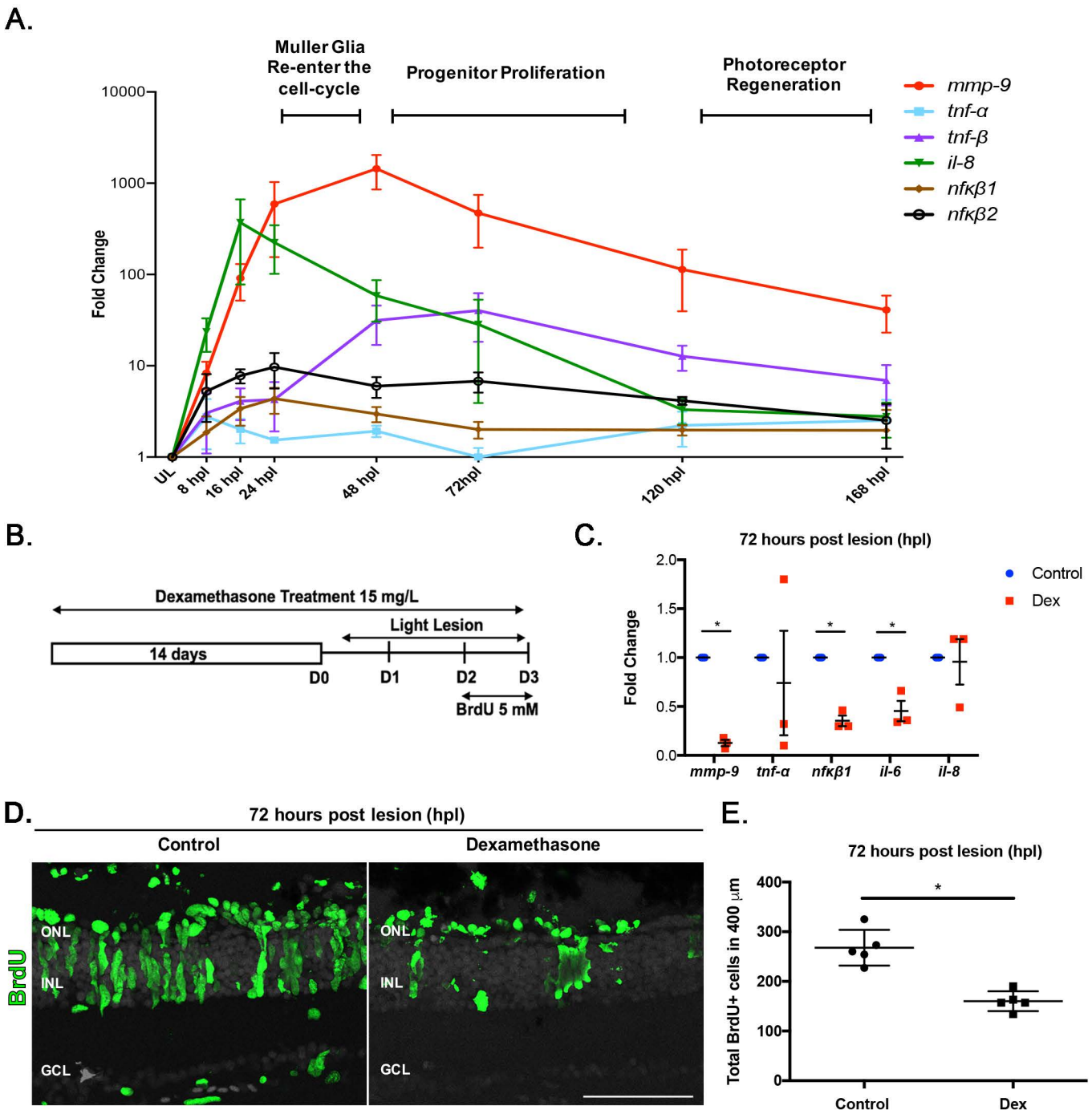
A.
Muller Glia Re-enter the cell-cycle
Progenitor Proliferation
Photoreceptor Regeneration
mmp-9
tnf-α
tnf-β
il-8
nfκβ1
nfκβ2
Fold Change
10000
1000
100
10
1
UL
8 hpl
16 hpl
24 hpl
48 hpl
72hpl
120 hpl
168 hpl
B.
Dexamethasone Treatment 15 mg/L
Light Lesion
14 days
D0
D1
D2
D3
BrdU 5 mM
C.
72 hours post lesion (hpl)
Control
Dex
Fold Change
2.0
1.5
1.0
0.5
0.0
mmp-9
tnf-α
nfκβ1
il-6
il-8
D.
72 hours post lesion (hpl)
Control
Dexamethasone
BrdU
ONL
INL
GCL
E.
72 hours post lesion (hpl)
Total BrdU+ cells in 400 μm
400
300
200
100
0
Control
Dex

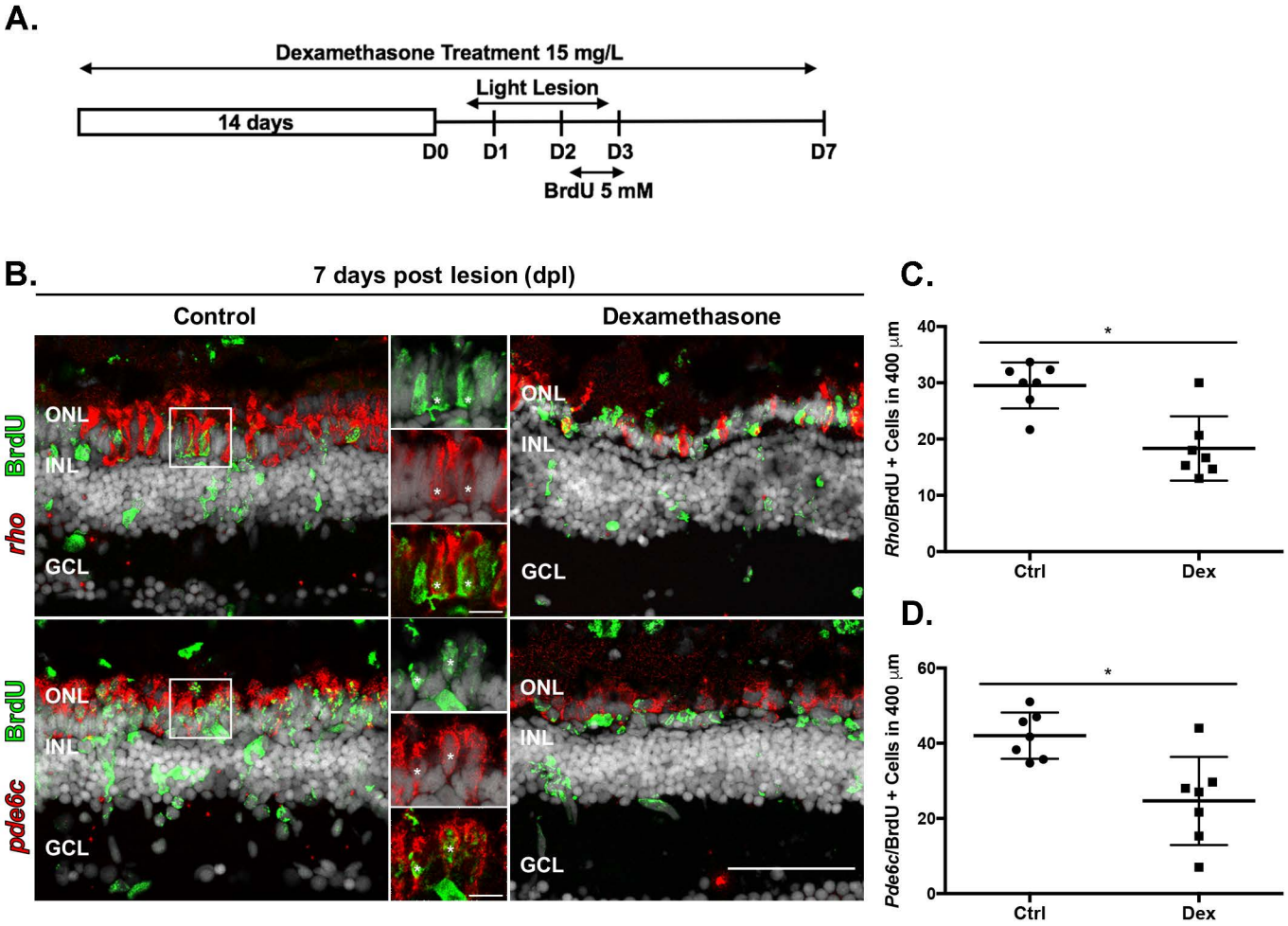
A.
Dexamethasone Treatment 15 mg/L
Light Lesion
14 days
D0
D1
D2
D3
D7
BrdU 5 mM
B.
7 days post lesion (dpl)
Control
Dexamethasone
BrdU
rho
ONL
INL
GCL
BrdU
pde6c
ONL
INL
GCL
C.
Rho/BrdU + Cells in 400 µm
40
30
20
10
0
*
Ctrl
Dex
D.
Pde6c/BrdU + Cells in 400 µm
60
40
20
0
*
Ctrl
Dex

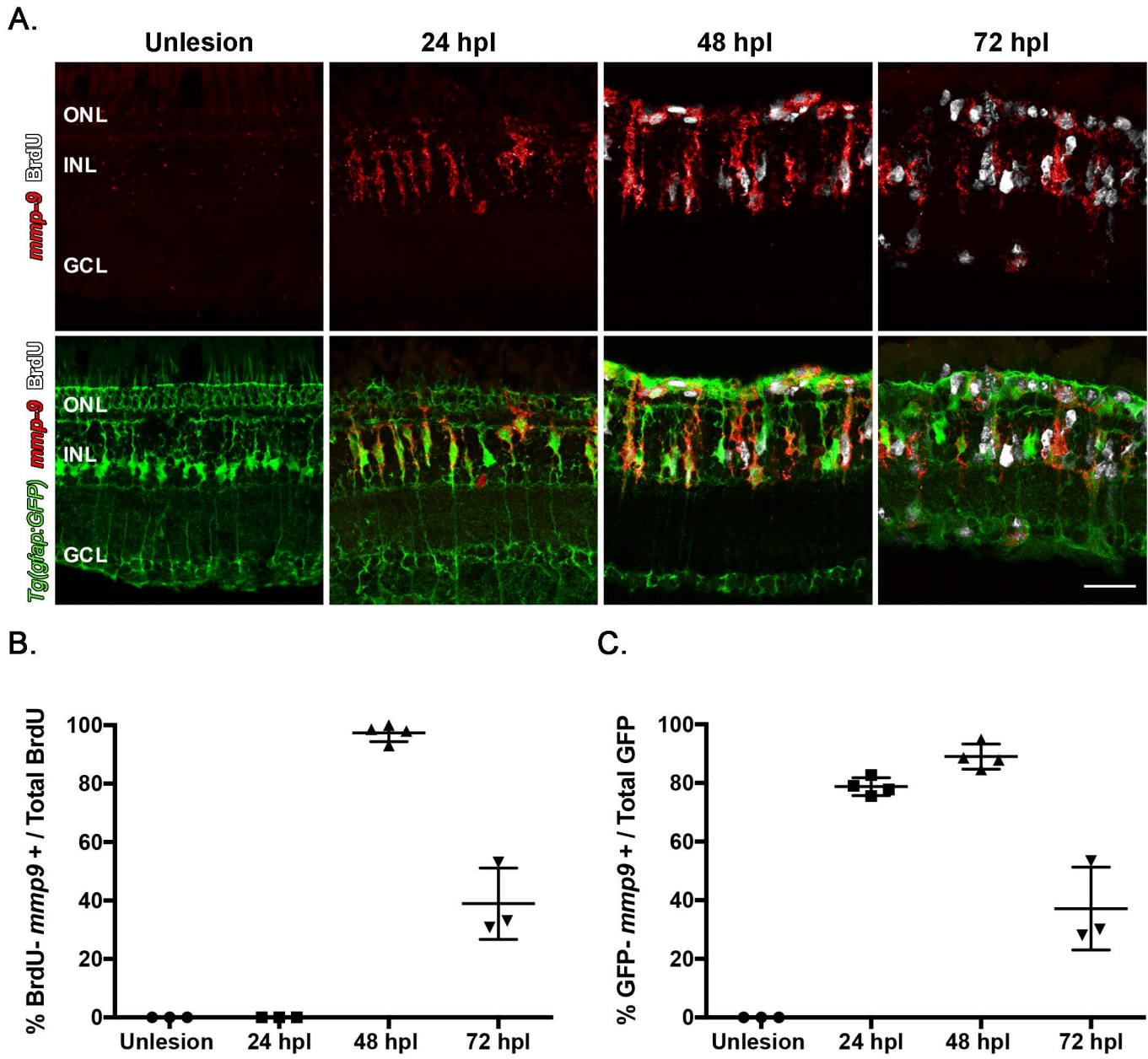
A.
Unlesion
24 hpl
48 hpl
72 hpl
ONL
INL
GCL
BrdU
mmp-9
Tg(gfap:GFP)
B.
% BrdU- mmp9 + / Total BrdU
100
80
60
40
20
0
Unlesion
24 hpl
48 hpl
72 hpl
C.
% GFP- mmp9 + / Total GFP
100
80
60
40
20
0
Unlesion
24 hpl
48 hpl
72 hpl

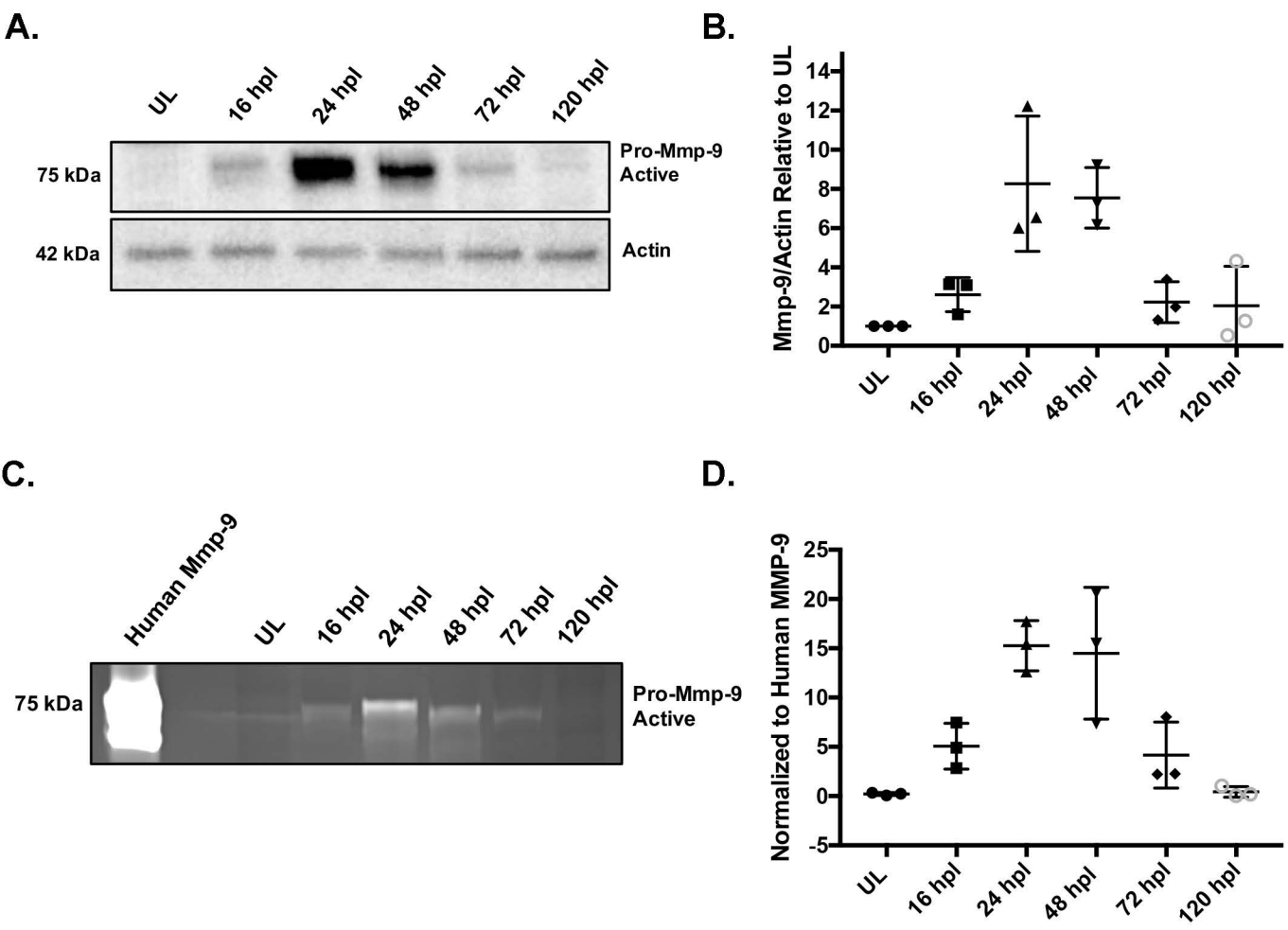
A.
UL
16 hpl
24 hpl
48 hpl
72 hpl
120 hpl
75 kDa
42 kDa
Pro-Mmp-9
Active
Actin
B.
Mmp-9/Actin Relative to UL
14
12
10
8
6
4
2
0
UL
16 hpl
24 hpl
48 hpl
72 hpl
120 hpl
C.
Human Mmp-9
UL
16 hpl
24 hpl
48 hpl
72 hpl
120 hpl
75 kDa
Pro-Mmp-9
Active
D.
Normalized to Human MMP-9
25
20
15
10
5
0
-5
UL
16 hpl
24 hpl
48 hpl
72 hpl
120 hpl

A.

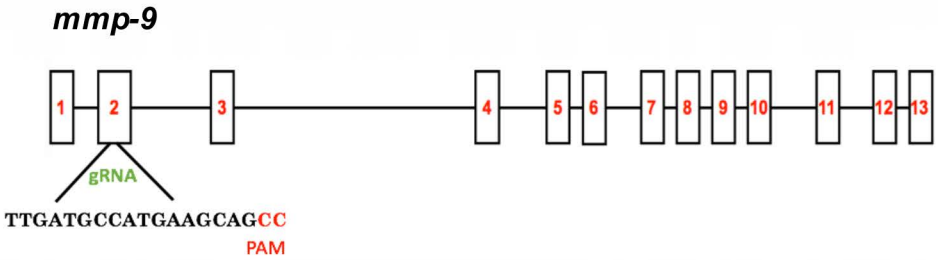
mmp-9
1
2
3
4
5
6
7
8
9
10
11
12
13
gRNA
TTGATGCCATGAAGCAGCC
PAM

B.

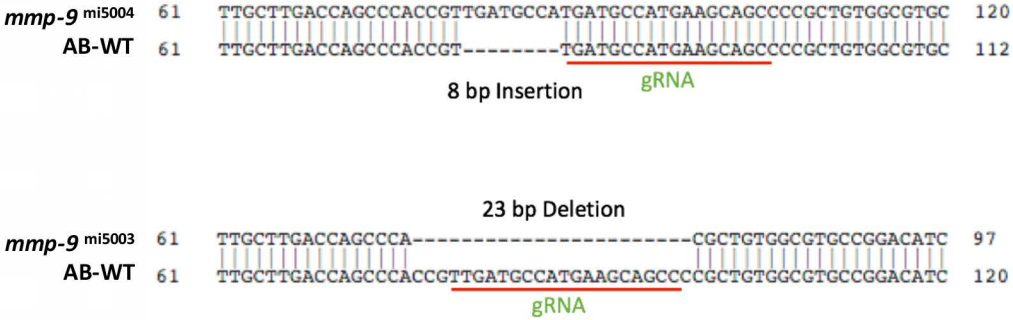
mmp-9 mi5004 61 TTGCTTGACCAGCCCACCGTTGATGCCATGATGCCATGAAGCAGCCCCGCTGTGGCGTGC 120
AB-WT 61 TTGCTTGACCAGCCCACCGT---------TGATGCCATGAAGCAGCCCCGCTGTGGCGTGC 112
8 bp Insertion
gRNA
23 bp Deletion
mmp-9 mi5003 61 TTGCTTGACCAGCCCA----------CGCTGTGGCGTGCCGGACATC 97
AB-WT 61 TTGCTTGACCAGCCCACCGTTGATGCCATGAAGCAGCCCCGCTGTGGCGTGCCGGACATC 120
gRNA

C.

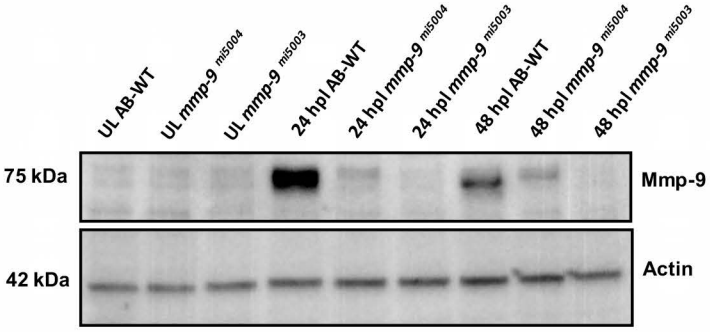
UL AB-WT
UL mmp-9 mi5004
UL mmp-9 mi5003
24 hpl AB-WT
24 hpl mmp-9 mi5004
24 hpl mmp-9 mi5003
48 hpl AB-WT
48 hpl mmp-9 mi5004
48 hpl mmp-9 mi5003
75 kDa
Mmp-9
42 kDa
Actin

D.

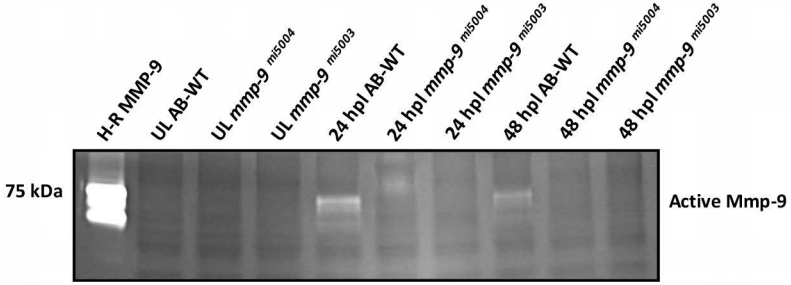
H-R MMP-9
UL AB-WT
UL mmp-9 mi5004
UL mmp-9 mi5003
24 hpl AB-WT
24 hpl mmp-9 mi5004
24 hpl mmp-9 mi5003
48 hpl AB-WT
48 hpl mmp-9 mi5004
48 hpl mmp-9 mi5003
75 kDa
Active Mmp-9

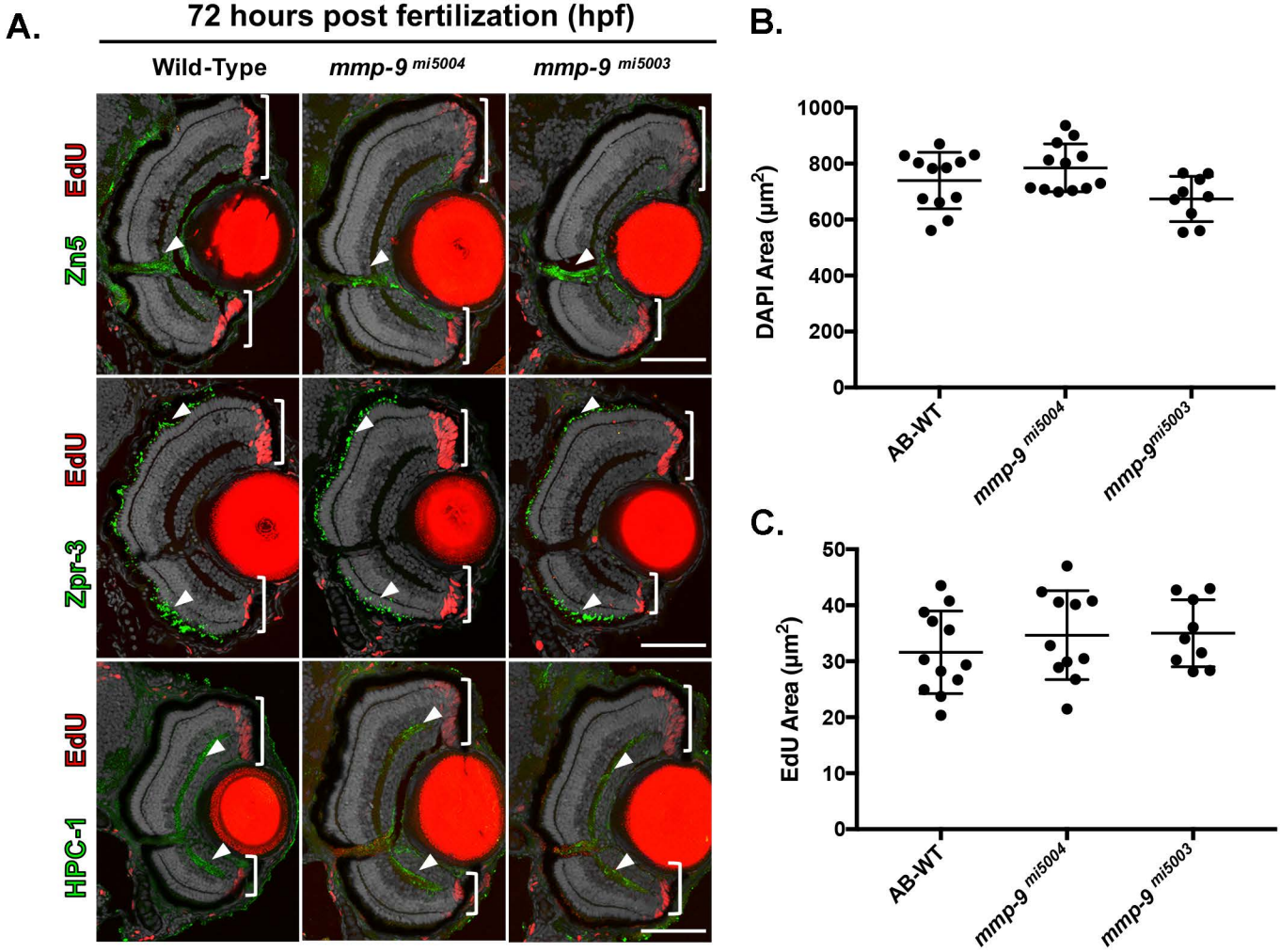
A.
72 hours post fertilization (hpf)
Wild-Type
mmp-9 mi5004
mmp-9 mi5003
EdU
Zn5
EdU
Zpr-3
EdU
HPC-1
B.
DAPI Area (µm2)
1000
800
600
400
200
0
AB-WT
mmp-9 mi5004
mmp-9mi5003
C.
EdU Area (µm2)
50
40
30
20
10
0
AB-WT
mmp-9 mi5004
mmp-9 mi5003

A.

Unlesion (UL) Adults

AB-WT | *mmp-9* mi5004 | *mmp-9* mi5003

Lee's Stain

ONL

INL

GCL

B.

Unlesion

Wild-Type | *mmp-9* mi5003

Zpr-1

BrdU

ONL

INL

GCL

D.

72 hours post lesion

Wild-Type | *mmp-9* -/- TH

BrdU

Hoechst

ONL

INL

GCL

C.

ZRF-1 + cells in 500 μm

65

60

55

50

45

AB-WT | *mmp-9* mi5003

BrdU+ cells in 500 μm

8

6

4

2

0

AB-WT | *mmp-9* mi5003

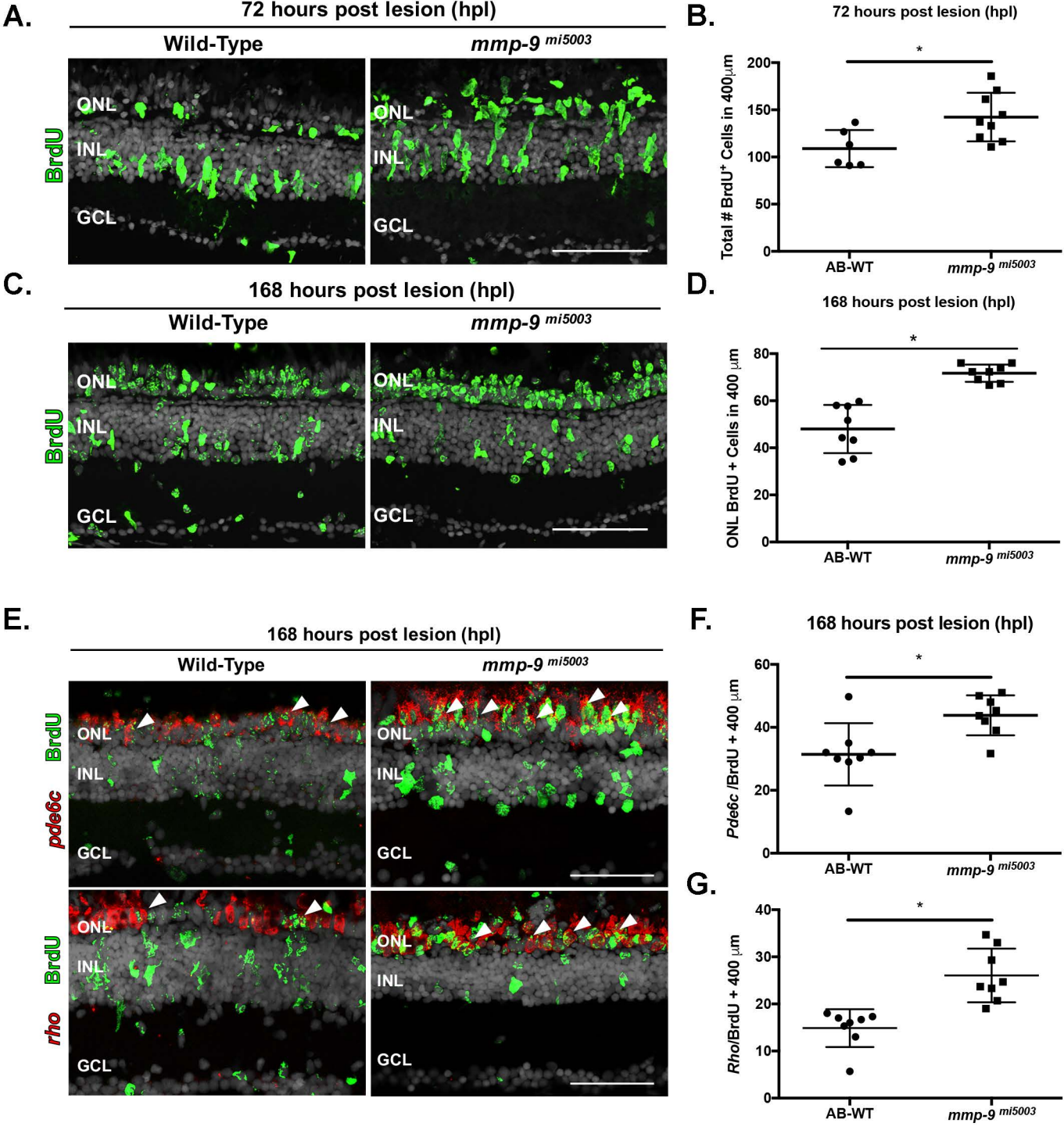
A.
72 hours post lesion (hpl)
Wild-Type
mmp-9 mi5003
BrdU
ONL
INL
GCL
B.
72 hours post lesion (hpl)
Total # BrdU+ Cells in 400µm
200
150
100
50
0
*
AB-WT
mmp-9 mi5003
C.
168 hours post lesion (hpl)
Wild-Type
mmp-9 mi5003
BrdU
ONL
INL
GCL
D.
168 hours post lesion (hpl)
ONL BrdU + Cells in 400 µm
80
60
40
20
0
*
AB-WT
mmp-9 mi5003
E.
168 hours post lesion (hpl)
Wild-Type
mmp-9 mi5003
BrdU
pde6c
rho
ONL
INL
GCL
F.
168 hours post lesion (hpl)
Pde6c /BrdU + 400 µm
60
40
20
0
*
AB-WT
mmp-9 mi5003
G.
Rho/BrdU + 400 µm
40
30
20
10
0
*
AB-WT
mmp-9 mi5003

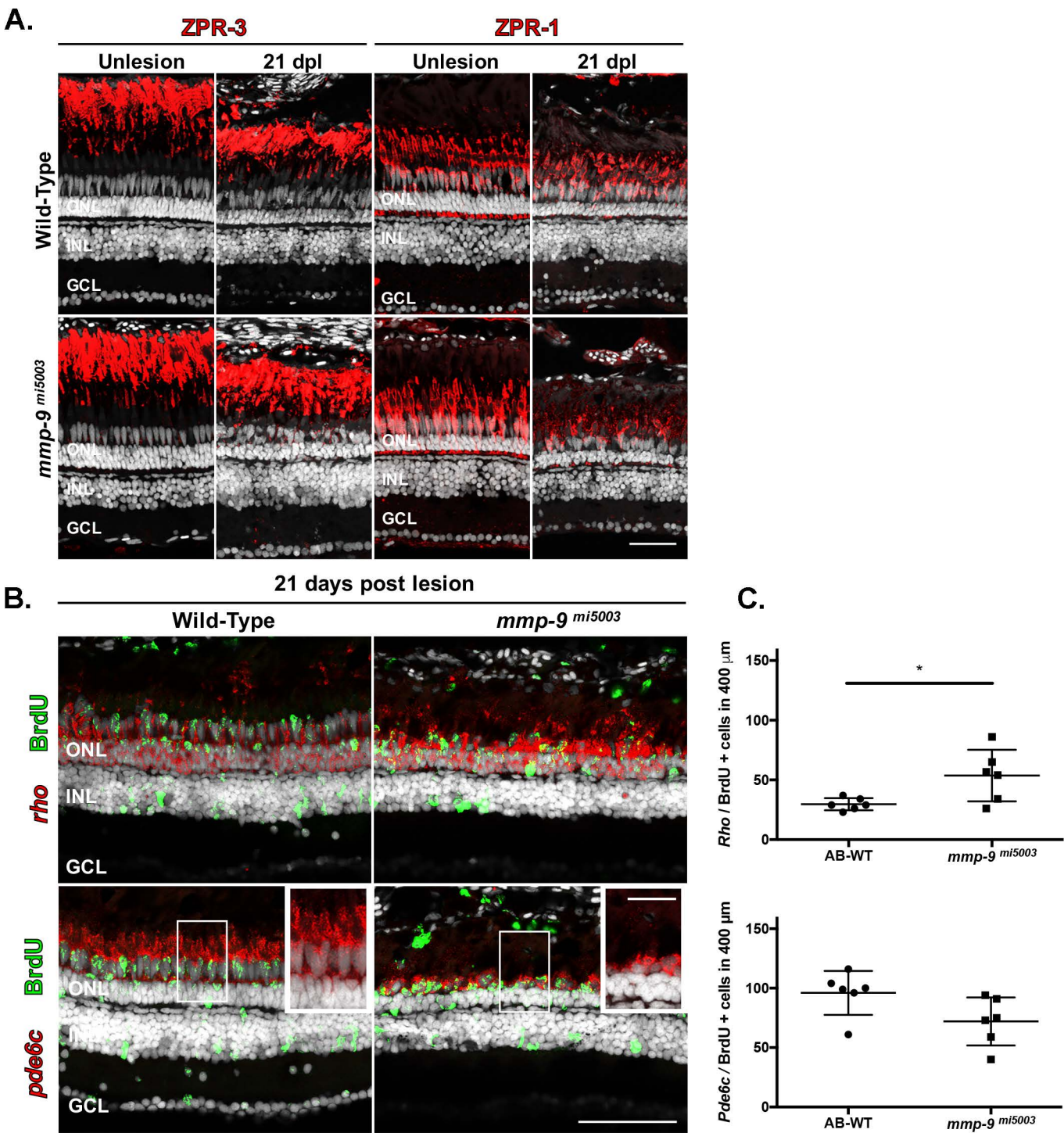
A.
ZPR-3
ZPR-1
Unlesion
21 dpl
Unlesion
21 dpl
Wild-Type
mmp-9 mi5003
ONL
INL
GCL
B.
21 days post lesion
Wild-Type
mmp-9 mi5003
BrdU
rho
pde6c
C.
Rho / BrdU + cells in 400 µm
Pde6c / BrdU + cells in 400 µm
150
100
50
0
*
AB-WT
mmp-9 mi5003

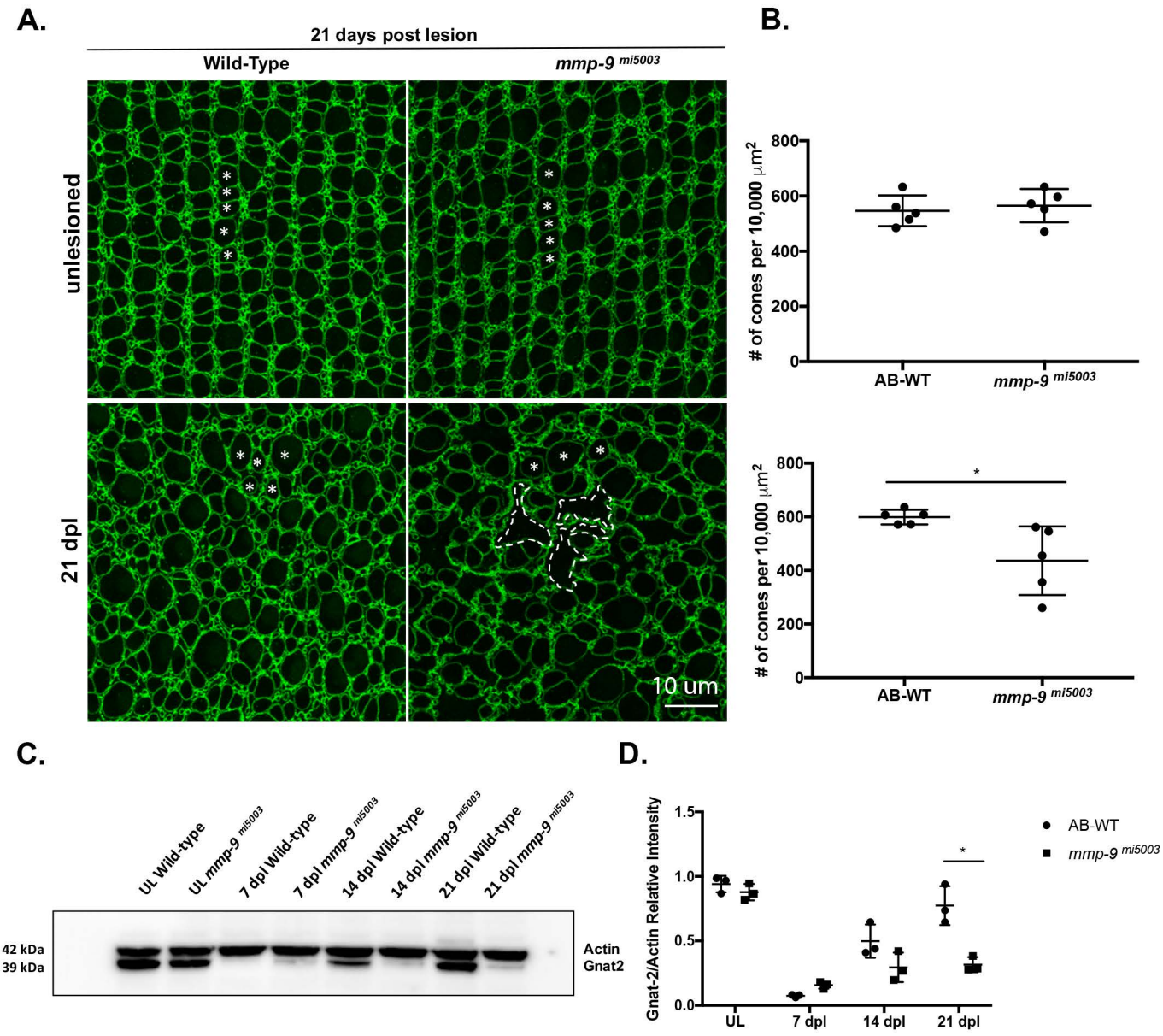
A.
21 days post lesion
Wild-Type
mmp-9 mi5003
unlesioned
21 dpl
10 um
B.
# of cones per 10,000 μm2
800
600
400
200
0
AB-WT
mmp-9 mi5003
*
C.
UL Wild-type
UL mmp-9 mi5003
7 dpl Wild-type
7 dpl mmp-9 mi5003
14 dpl Wild-type
14 dpl mmp-9 mi5003
21 dpl Wild-type
21 dpl mmp-9 mi5003
42 kDa
39 kDa
Actin
Gnat2
D.
Gnat-2/Actin Relative Intensity
1.5
1.0
0.5
0.0
UL
7 dpl
14 dpl
21 dpl
AB-WT
mmp-9 mi5003
*

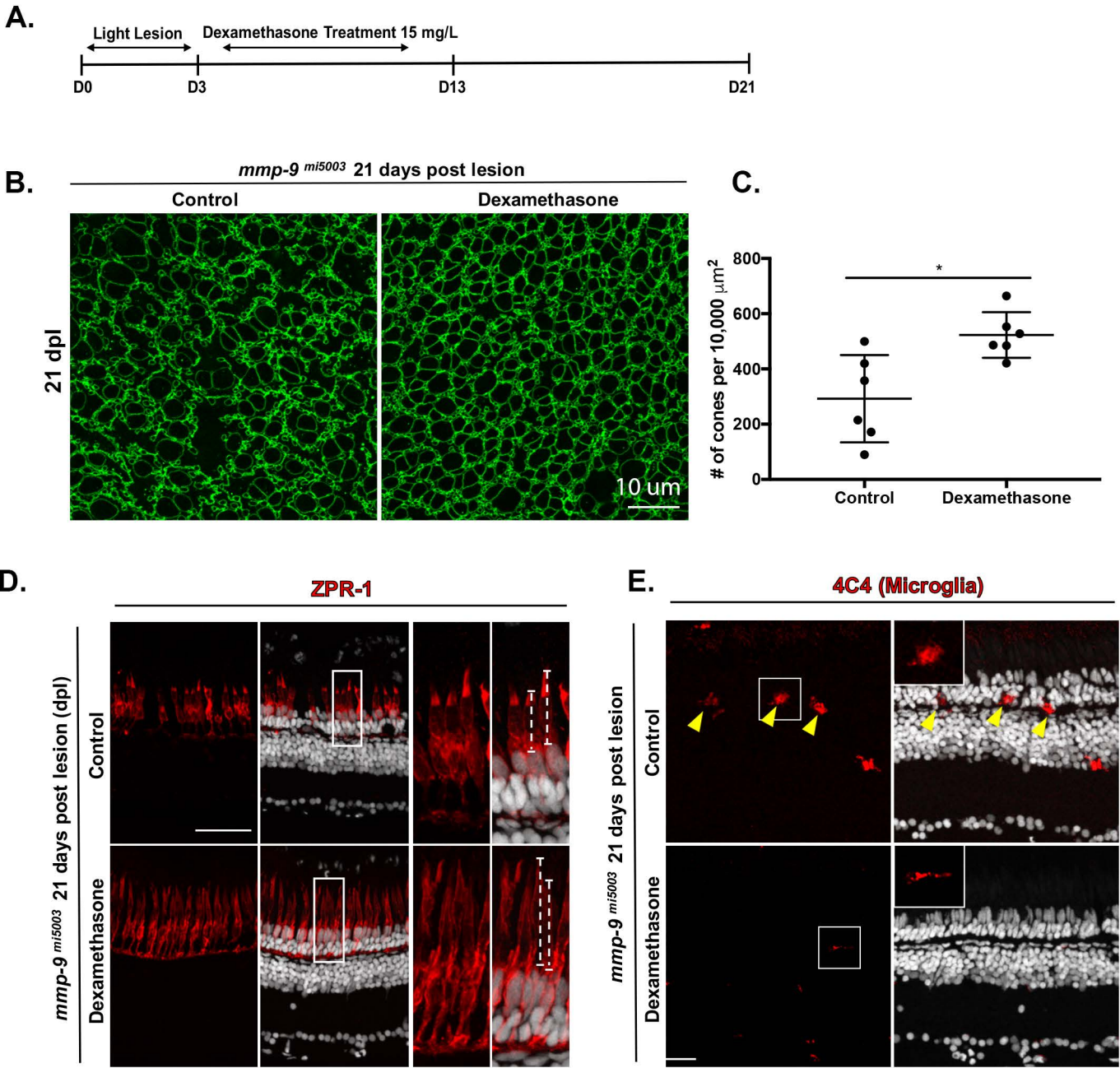
A.
Light Lesion
Dexamethasone Treatment 15 mg/L
D0
D3
D13
D21
B.
mmp-9 mi5003 21 days post lesion
Control
Dexamethasone
21 dpl
10 um
C.
# of cones per 10,000 μm2
800
600
400
200
0
*
Control
Dexamethasone
D.
ZPR-1
mmp-9 mi5003 21 days post lesion (dpl)
Control
Dexamethasone
E.
4C4 (Microglia)
mmp-9 mi5003 21 days post lesion
Control
Dexamethasone

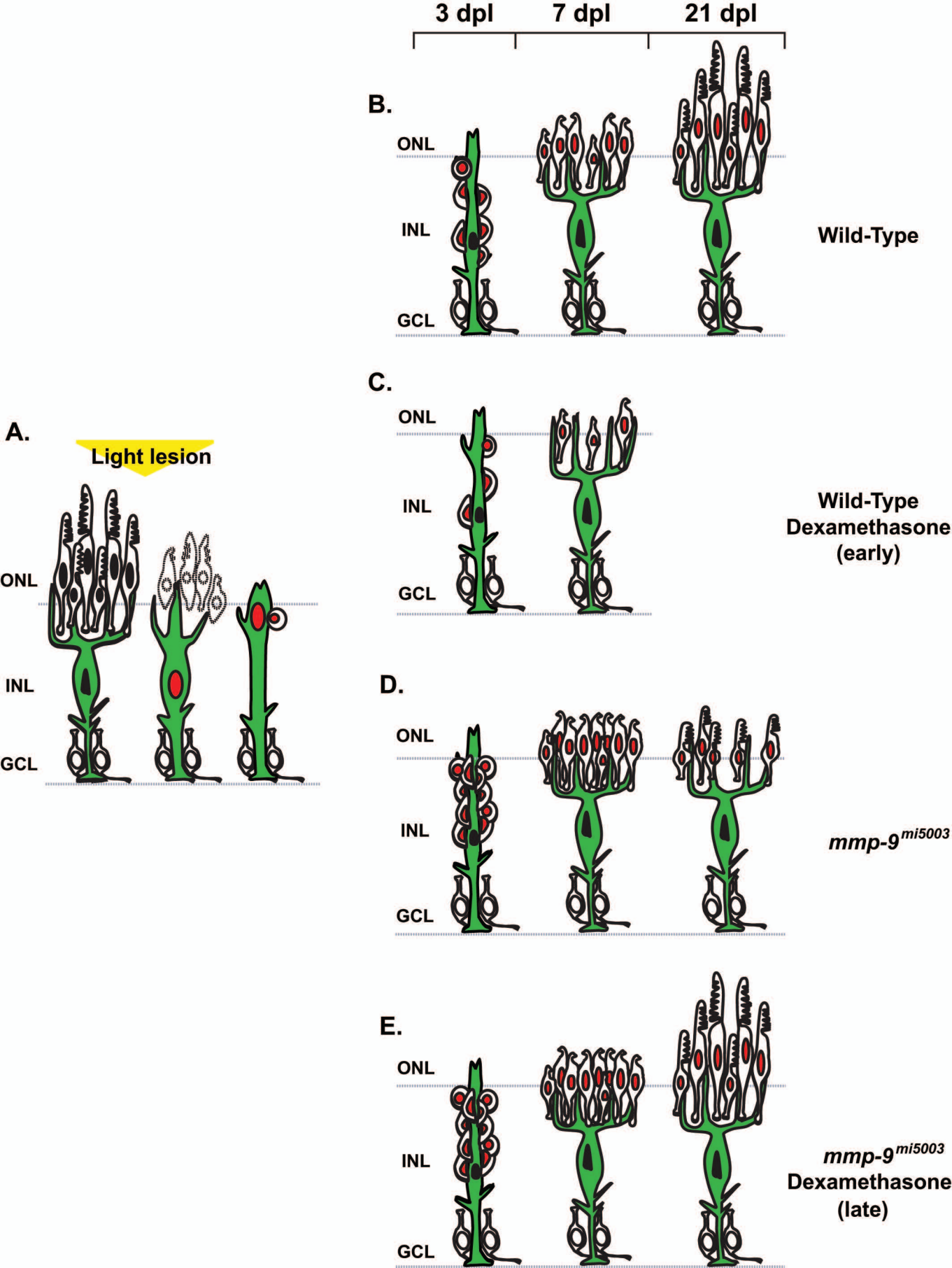
3 dpl
7 dpl
21 dpl
B.
ONL
INL
GCL
Wild-Type
C.
ONL
INL
GCL
Wild-Type
Dexamethasone
(early)
A.
Light lesion
ONL
INL
GCL
D.
ONL
INL
GCL
mmp-9mi5003
E.
ONL
INL
GCL
mmp-9mi5003
Dexamethasone
(late)

```
Mmp9          MRLGVLAFLVLGTCSLRAWCLPLKSVFVTFPGDVIKNMTNTQLADEYLKRYGYVDVLQRS
Mmp9mi5003    MRLGVLAFLVLGTCSLRAWCLPLKSVFVTFPGDVIKNMTNTQLADEYLKRYGYVDVLQRS
Mmp9mi5004    MRLGVLAFLVLGTCSLRAWCLPLKSVFVTFPGDVIKNMTNTQLADEYLKRYGYVDVLQRS

Mmp9          GLQAVISNAKALKKLQRQLGLEETGLLDQPTVDAMKQPRCGVPDIRNYKTFDGDLKWDHT
Mmp9mi5003    GLQAVISNAKALKKLQRQLGLEETGLLDQPTLWRAGHPQLQDIRRRPEVGSHRCHIQDFE
Mmp9mi5004    GLQAVISNAKALKKLQRQLGLEETGLLDQPTVDAMMP-----------------------

Mmp9          DVTYRILNYSPDMEASLIDDAFARAFKVWSDVTPLTFTRLFDGIADIMISFGKLDHGDPY
Mmp9mi5003    LFARHGSLFDR--------------------------------------------------
Mmp9mi5004    ------------------------------------------------------------

Mmp9          PFDGKDGLLAHAYPPGEGTQGDAHFDDDEYWTLGSGPAIQTRYGNAEGAMCHFPFLFEGT
              SYSTCTTEGRTDGLPWCSTTADYDKDKKFGFCPSELLFTFDGNSNEAPCVFPFVFDGKKY
              DSCTTEGRNDGYRWCSTTANFDTDKKYGFCPNRDTAVIGGNSEGEPCHFPFTFLGNTYSS
              CTSEGRNDGKLWCGTTSNYDTDKKWGFCPDRGYSLFLVAAHEFGHALGLDHSNIKDALMY
              PMYKYVEGFPLHRDDIDGIQYLYGPRTGPEPTAPQPRTTTSSPVVPTKPSPSDKTTTAST
              TTQVVPSDDACQIKEFDAITEIQKELHFFKDGRYWKISGNGERKGPFMISAKWPALPAVI
              NSAFEDHLTKKIYFFSERQFWVYSGNDVLGPRKIEKLGLPSDLDKVEGSMQRGKGKVLLF
              NGENFWRLDVKAQLIDRGYPRFTDAAFGGVPIDSHDVFLYKGFFYFCRESFYWRMNAKRQ
              VDRVGYVKYDLLKCSDIHSL
```